Atmos. Chem. Phys., 14, 2987–3015, 2014
www.atmos-chem-phys.net/14/2987/2014/
doi:10.5194/acp-14-2987-2014

Atmospheric Chemistry and Physics Open Access

Further evidence of important environmental information content in red-to-green ratios as depicted in paintings by great masters

C. S. Zerefos[1,2], P. Tetsis[1], A. Kazantzidis[3], V. Amiridis[4], S. C. Zerefos[5], J. Luterbacher[6], K. Eleftheratos[7], E. Gerasopoulos[2,8], S. Kazadzis[8], and A. Papayannis[9]

[1]Academy of Athens, Athens, Greece
[2]Navarino Environmental Observatory (N.E.O.), Messinia, Greece
[3]Laboratory of Atmospheric Physics, Physics Department, University of Patras, Greece
[4]Institute of Astronomy, Astrophysics, Space Application and Remote Sensing, National Observatory of Athens, Greece
[5]Hellenic Open University, Patras, Greece
[6]Department of Geography, Climatology, Climate Dynamics and Climate Change, Justus Liebig University of Giessen, Giessen, Germany
[7]Faculty of Geology and Geoenvironment, University of Athens, Greece
[8]Institute of Environmental Research and Sustainable Development, National Observatory of Athens, Greece
[9]National Technical University of Athens, Athens, Greece

Correspondence to: C. S. Zerefos (zerefos@geol.uoa.gr)

Received: 11 November 2013 – Published in Atmos. Chem. Phys. Discuss.: 18 December 2013
Revised: 21 February 2014 – Accepted: 1 March 2014 – Published: 25 March 2014

Abstract. We examine sunsets painted by famous artists as proxy information for the aerosol optical depth after major volcanic eruptions. Images derived from precision colour protocols applied to the paintings were compared to online images, and found that the latter, previously analysed, provide accurate information. Aerosol optical depths (AODs) at 550 nm, corresponding to Northern Hemisphere middle latitudes, calculated by introducing red-to-green (R / G) ratios from a large number of paintings to a radiative transfer model, were significantly correlated with independent proxies from stratospheric AOD and optical extinction data, the dust veil index, and ice core volcanic indices. AODs calculated from paintings were grouped into 50-year intervals from 1500 to 2000. The year of each eruption and the 3 following years were defined as "volcanic". The remaining "non-volcanic" years were used to provide additional evidence of a multidecadal increase in the atmospheric optical depths during the industrial "revolution". The increase of AOD at 550 nm calculated from the paintings grows from 0.15 in the middle 19th century to about 0.20 by the end of the 20th century. To corroborate our findings, an experiment was designed in which a master painter/colourist painted successive sunsets during and after the passage of Saharan aerosols over the island of Hydra in Greece. Independent solar radiometric measurements confirmed that the master colourist's R / G ratios which were used to model his AODs, matched the AOD values measured in situ by co-located sun photometers during the declining phase of the Saharan aerosol. An independent experiment was performed to understand the difference between R / G ratios calculated from a typical volcanic aerosol and those measured from the mineral aerosol during the Hydra experiment. It was found that the differences in terms of R / G ratios were small, ranging between −2.6 % and +1.6 %. Also, when analysing different parts of cloudless skies of paintings following major volcanic eruptions, any structural differences seen in the paintings had not altered the results discussed above. However, a detailed study on all possible sources of uncertainties involved (such as the impact of clouds on R / G ratios) still needs to be studied. Because of the large number of paintings studied, we tentatively propose the conclusion that regardless of the school, red-to-green ratios from great masters can provide independent proxy AODs that correlate with widely accepted proxies and with independent measurements.

Published by Copernicus Publications on behalf of the European Geosciences Union.

1 Introduction

In the paper by Zerefos et al. (2007), the monochromatic ratios between red, green and blue colours, in paintings before, during and after large volcanic eruptions were examined. In that study, digital images from 554 paintings were downloaded from the websites of several art galleries and museums. These images were processed to derive ratios between the intensities of monochromatic colours. For the calculation of the R / G ratios only the parts of the sky over the field of view of the artist near the horizon avoiding clouds were analysed. The average values and the standard deviation of R / G ratio for each painting were presented in Appendix B of Zerefos et al. (2007). In that study, the mean error value was 0.014 due to the variability of R / G ratios within the paintings/images. That variability and how it could affect the estimated AOD values for different aerosol conditions and solar zenith angles was examined. The uncertainty found was less than 0.05 for small optical depths and smaller SZA (70°). The error increased with increasing AOD and SZA (85°) and could be as large as 0.18 for AOD values exceeding 0.5. The study by Zerefos et al. (2007) concluded that regardless of the school or the style of the painter, the R / G ratios at low solar elevation angles, correlated well to the modelled aerosol optical depth (AOD) values following large volcanic eruptions. After its publication we were faced with the dilemma that the various digital images available at the above-mentioned websites were not necessarily accurate representations of the true colour profile reproduction, because they were not created following a single colour profile protocol and thus, we decided to revisit the issue.

In this work we provide new evidence that our earlier results, based on R / G ratios to estimate and model AODs in paintings are robust, a hypothesis which is supported using the following three methods: firstly, by correlating the available R / G ratios from the above-mentioned public websites with the same ratios from their respective high quality colour profile protocols. A colour profile protocol is the protocol (set of instructions) used to accurately translate colour through different devices. In our work a colour profile was absolutely necessary so that the scanned paintings retained their original colour information when distributed through digital means. Also by having the colour profile along with calibrated scanners it was possible to compare paintings from other colourists without any uncertainty by differences due to colour translation. Secondly, by comparing our earlier results of AODs based on art, with results and indices from other proxies (ice cores, pyrheliometric and other data) which cover the past 500 years (Lamb, 1970, 1977, 1983; Sato et al., 1993; Stothers, 1996, 2001; Robertson et al., 2001; Gao et al., 2008; Crowley and Unterman, 2013). Thirdly, by performing an experiment involving the creation of sunset paintings and then measuring the ratios of the art piece with collocated AOD measurements actually recorded in the atmosphere during and after the passage of a Saharan dust event.

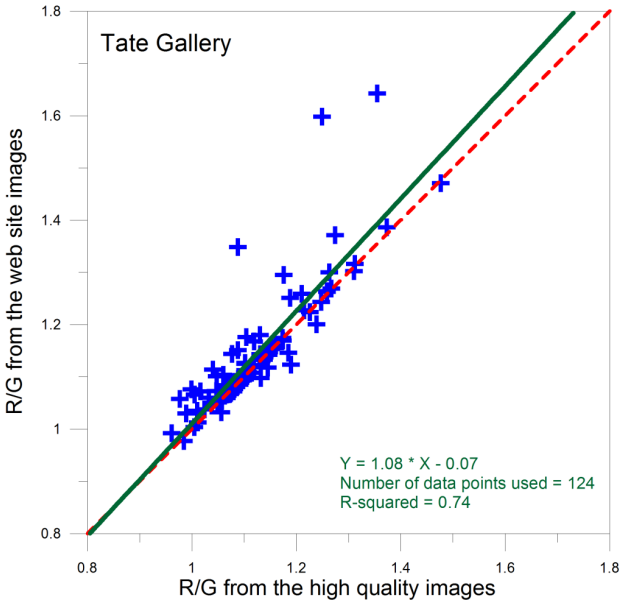

Fig. 1. R / G ratios derived from painting digital images from web site (low resolution) vs. R / G ratios for the same paintings obtained through colour profile protocol (high resolution) at the Tate Gallery. The corresponding linear best fit (green line) and the perfect correlation line (dashed red line) are also shown. The values correspond to the 124 landscape paintings listed in Appendix A.

More specifically, we have organized an experimental campaign where Panayiotis Tetsis[1] (a well-known Greek landscape painter and colourist) painted the sunsets at the Hydra island in the Aegean Sea, during and after the passage of a Saharan dust event on the 19 and 20 June 2010. During the creation of the paintings, we performed simultaneous measurements of the evolution of the observed AODs and the actual meteorological conditions were carefully monitored. The results from these three methods are described below.

2 Comparison between high and low quality digital images of paintings

As mentioned in the introduction, in an earlier study (Zerefos et al., 2007) the vast majority of images were analysed from museum web sites which were not created following a rigorous colour profile protocol. The method of painting sampling and an analysis of the corresponding uncertainties is described in the study by Zerefos et al. (2007). Since it was not possible to obtain high quality images of paintings from all galleries, we focus here on the subset kept at the Tate Gallery in the United Kingdom (UK). At this gallery we found 124 digital images of paintings (with a 300 dpi resolution, RGB, 8 bit compressed jpeg format files) which were also analysed in our earlier work (listed in Appendix A).

[1] http://www.wikipaintings.org/en/panayiotis-tetsis

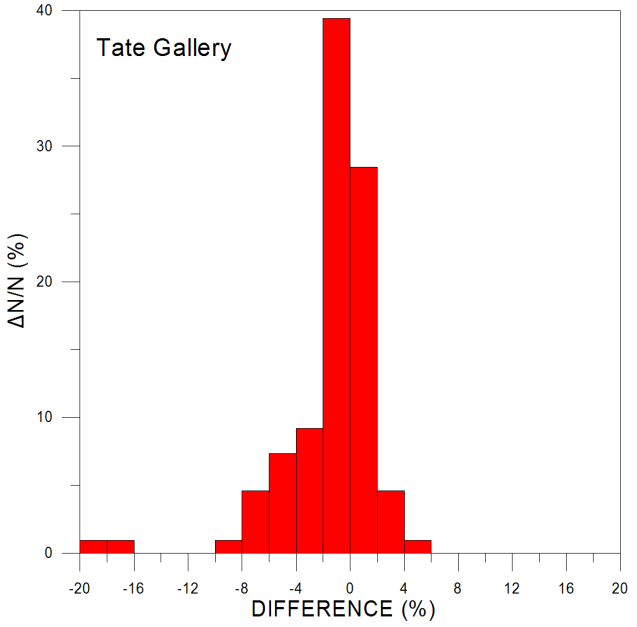

Fig. 2. Distribution of the relative differences (in %) between the R / G ratios derived from the high- and the low-resolution images from 124 landscape sunsets at the Tate Gallery (listed in Appendix A).

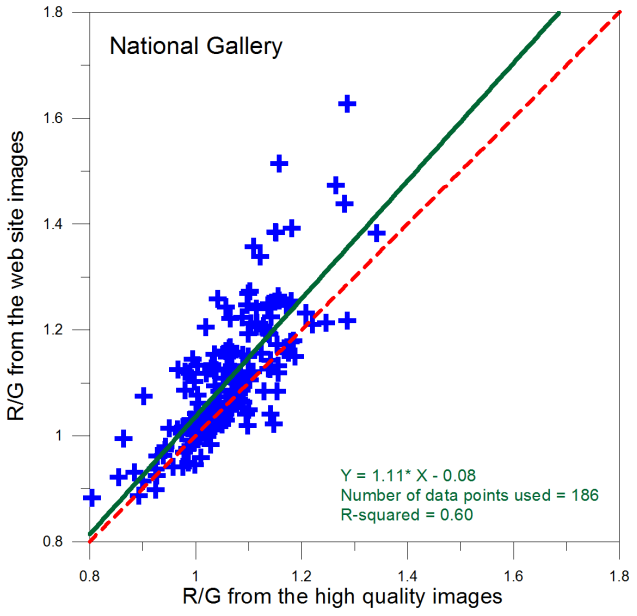

Fig. 3. Results from a completely independent sample of paintings. R / G ratios derived from painting digital images from the web site (low resolution) vs. the same R / G ratios from high resolution digital images at the National Gallery, London. The corresponding linear fit (green line) and the $y = x$ line (dashed red line) are also shown. The values correspond to 186 landscape paintings, which were not used in the early study by Zerefos et al. (2007), as described in the text.

Figure 1 shows the results of the R / G values retrieved from these high quality images in comparison to the ratios (calculated for the same paintings) from the website images, using the same methodology, as described in Zerefos et al. (2007). As can be seen from Fig. 1, the difference between the R / G values of the lower and higher resolution digital images stays within ± 4 % for almost all paintings. Very few exceptions with overestimations correspond to solar zenith angles exceeding 90°.

This result is clearly seen in Fig. 2 which shows the percent distribution of the relative differences between the R / G ratios derived from the high vs. the low resolution 124 images from the Tate Gallery.

Additionally, an independent sample of 186 landscape paintings of high quality/resolution (10000×10000 pixel images), covering the 1500–1900 time period, obtained from the National Gallery, London, calibrated using the Gretag Macbeth 24-patch colour rendition chart (Saunders et al., 2002; McCamy et al., 1976). None of these paintings has been studied in our earlier study because they did not fulfil the selection criteria set, that is, for representing sunsets and the possibility for direct or indirect measurements through clear shades, to facilitate the estimate of solar zenith angle, pertaining to each painting.

The high-quality/resolution images obtained directly from the National Gallery were next compared to their corresponding low-quality/resolution images obtained from the website (http://www.nationalgallery.org.uk/cgi-bin/WebObjects.dll/CollectionPublisher) to test further the results obtained from the Tate Gallery comparisons shown in Figs. 1 and 2.

The retrieved R / G values of these images are shown in Fig. 3, from which we see that on the average, the R / G values are overestimated by 0.04 ± 0.08. This result is in agreement with the results from the Tate Gallery sample of paintings and a tentative result is that the overestimation is larger (up to 0.3) deviating from the linear fit for the higher R / G values. At any rate, the correlation coefficients are still highly significant (99 % confidence level). It should be noted here that all images in this study were processed with the "nip2" software (e.g. http://www.vips.ecs.soton.ac.uk/index.php?title=Nip2) which comfortably works with multi-gigabyte images. A special work script has been created in order to calculate the average R / G values of the sky from each painting, as derived from the low- and high-quality/resolution images.

3 Other factors that might affect the R / G ratios from paintings

When trying to estimate a number that would describe the true colour at given solar zenith angle during a sunset, there are several factors that are important sources of uncertainty. Among them are the coatings, the degradation of colour due

to ageing, the unknown systematic practices used by the painters, the mood of the painter and the different styles of schools. However, we have to keep in mind that the earlier and present findings, of a relation between high aerosol content at sunsets, were not based on true colours but confined only to the case of the R / G ratios. The different factors affecting the true colours mentioned above, being either random or systematic, may also affect the R / G ratios. Although this may be true for an individual painting, the statistics presented here show that when a large number of paintings by different painters are considered, these uncertainties could be much reduced. This is supported by the signal-to-noise ratio analysis of the statistical standard errors discussed in the introduction and in Zerefos et al. (2007). In addition, we have searched for a possible impact of structural differences. We provide here examples of paintings with and without structural differences following two major volcanic eruptions namely Tambora (1815) and Krakatau (1883). The calculated R / G ratios in parts of the sky give a similar result in which the differences are small, anyhow smaller than the standard errors we have encountered in this work (see paintings in Appendix C). Therefore, we have to tentatively assume that the impact of structural differences when studying R / G ratios in parts of the sky of the painting are small. We note here that we have made every possible effort to avoid measuring R / G ratios in the presence of clouds. It appears that R / G ratios as measured in this work somehow remind us of the ratios of solar irradiance in different wavelengths which are used in spectrophotometers to measure columnar gases in the atmosphere. In these spectroradiometers the noise introduced by aerosols and other factors related to scattering and related effects are indeed cancelled out and this is how we obtained the long series of total ozone, total sulfur dioxide, and total nitrogen dioxide with remarkably small standard error. We think that the reduction of errors when using R / G ratios provides useful information on the overhead aerosol content which correlates well when averaged with other proxies and/or with real AOD measurements as was the case with the Hydra experiment, discussed in paragraph 5.

In our study, a detailed quantification of each source of uncertainty was not possible except for the effects of quality in digitization of the paintings, structural differences and the solar zenith angle. Potential sources of uncertainty could be the atmospheric/aerosol related dynamics which affect the magnitude of the impact of each volcano in the area under study (of the painter) as well as the impact of cloudiness on the depicted R / G. We believe any effects from clouds have been avoided by trying to confine our R / G "measurements" to the cloudless parts of the sky in each painting. Following the above discussion and since our goal in this part of the manuscript was focused on the validation of the volcanic eruption effect and not on the actual quantification of the volcanic aerosol in the painting area, we believe that correlation coefficients with the mentioned proxies provide evidence that this goal has been achieved.

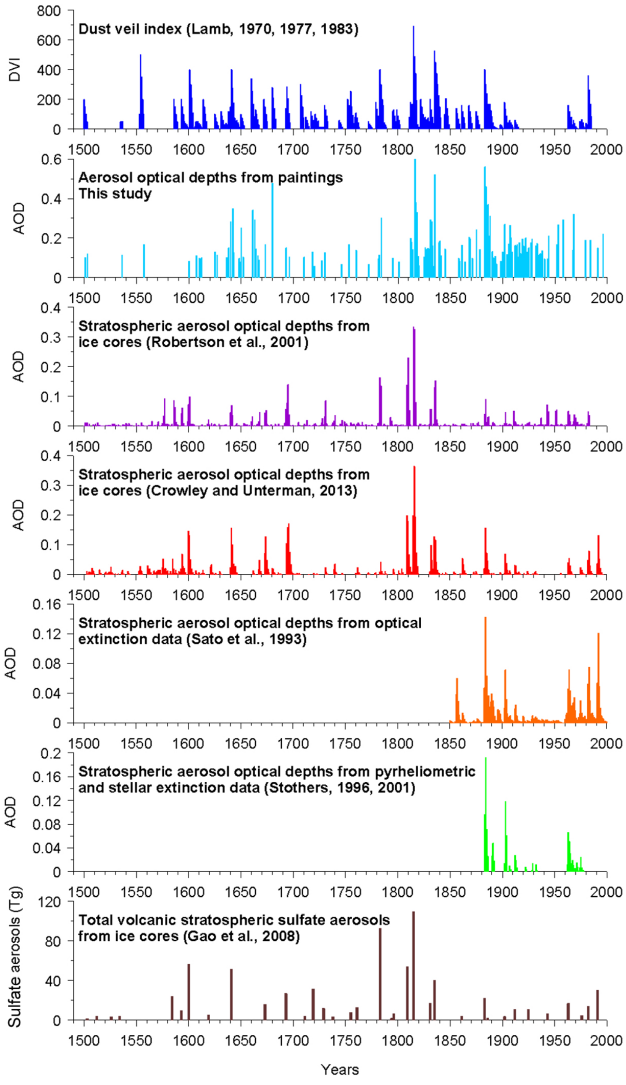

Fig. 4. Aerosol optical depth and other proxy indices during the past 500 years from different proxies (see text).

4 Atmospheric optical depths based on known proxies and on R / G ratios of paintings in the past 500 years

The earlier estimates of the aerosol optical depth at 550 nm (based on R / G calibrated ratios from paintings) and the radiative transfer model by Mayer and Kylling (2005) and Mayer and Emde (2007), were used to compile an independent time series with AODs during 1500–2000. Additionally, the time series of AODs calculated from paintings has been divided into 50-year intervals from 1500 to 2000. The year of each eruption and the 3 following years were defined as "volcanic". The remaining "non-volcanic" years were used to calculate the average AOD value pertaining to these years corresponding to Northern Hemisphere mid latitudes. This paper is based on evidence by western painters and colourists. The type of art is typical to western European

schools so it was inevitable to have more paintings in European countries. Nevertheless, the paper focuses on big volcanic eruptions that have an effect over the entire planet atmosphere, so the evidence could be noticed in most parts of the world. This long-term data set of AODs is compared to other independent proxies as shown in Fig. 4. Detailed information on those proxies can be found in the primary literature by Lamb (1970, 1977, 1983), Sato et al. (1993), Stothers (1996, 2001), Robertson et al. (2001), Gao et al. (2008) and Crowley and Unterman (2013). Using the data shown in Fig. 4, we found that the correlation coefficients between other proxy indices and the estimated AODs from the R / G ratios from paintings are statistically significant (Table 1). Appendix D presents the data used in the calculations shown in Table 1. The reader is also referred to the precision by which the extreme AODs between paintings and proxies during large volcanic eruptions match in most cases. In particular, in 102 cases for which data of both DVI and this study are simultaneously available, DVI spikes are coinciding with AOD spikes from this study at a percentage of 80 % (9 out of 11 cases). As spikes we define the values in both time series that belong in the upper 10 % range of values. In addition, this study revealed two high AOD cases that do not match with DVI spikes and it is worth noting that both failing cases succeeded a period of two consecutive years with spikes in both indices.

Total sulfate is the total measured sulfate concentration in ppb in the core, as resulted from deposition either from the stratosphere (volcanic) or the troposphere (anthropogenic and other biogenic sources), as described by Zielinski et al. (1996) and Robertson et al. (2001). The presented values do not refer directly to the atmospheric concentration, but rather to the deposition on ice which, however, is related to ambient concentrations. The values of calculated index of total sulfate from Greenland ice cores (Zielinski, 1995; Zielinski et al., 1996) and the longer time series of stratospheric AOD (Robertson et al., 2001) were grouped in 50-year time intervals with the same procedure described above for AODs calculated from paintings. The three data sets are presented in Fig. 5. We note here the point raised by Robertson et al. (2001) that the last 150-year increase in total sulfate from ice cores was hypothesized to be the result of tropospheric anthropogenic sulfate deposition. The point raised by Robertson et al. that there have been no major volcanic eruptions between 1900 and 1960, needs some clarification. Indeed in the list of major volcanic eruptions in the past 500 years (Appendix B after Ammann and Naveau, 2003; Robock, 2000), we can see that based on VEI two eruptions, Santa Maria (1903) and Katmai (1912) have been classified with VEI 6. However, VEI is known to be not a good index of stratospheric sulfate loading since it measures the explosivity of a volcano and not its stratospheric injection. A good example is the 1980 St. Helen's eruption, with a VEI of 5 but no stratospheric or climatic impact (A. Robock, personal communication, 2014). Stratospheric injection is important to ensure its global or hemispheric effects. From the above discussion it can be proposed that compared to the pre-industrial period, the industrial period shows higher painting-derived aerosol content, in agreement with what is expected from the literature (e.g. Neftel et al., 1985; Robock and Free, 1995; Robertson et al., 2001; Forster et al., 2007; Wild, 2012).

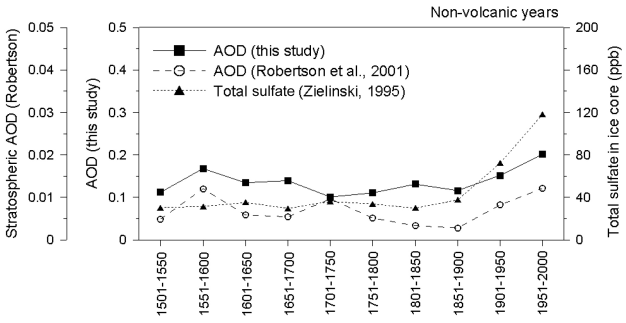

Fig. 5. Total AOD from paintings and in the stratosphere and total sulfate in Greenland ice core (in ppb) averaged over 50-year intervals for "non-volcanic" years during the period 1500–2000 AD.

5 A live case: the Hydra experiment

To corroborate our findings, a dedicated experimental campaign has been organized and implemented in Greece, aiming to evaluate the R / G retrieval methodology against ground-truth measurements of the aerosol load in terms of AOD values. The well-known colourist and landscape painter Panayiotis Tetsis (http://www.wikipaintings.org/en/panayiotis-tetsis) kindly offered to paint in real time a number of sunsets at the island of Hydra. As the great master was painting, a suite of ground-based aerosol measurements were collected, mainly by means of collocated sun photometry equipment. The master colourist had no idea of the passage of a Saharan dust cloud over Hydra.

5.1 Experiment organization and instrumentation

The experiment was conducted in Hydra, the painter's home base. Hydra is an island located in the Aegean Sea (37.21° N, 23.28° E), 80 km south of Athens, and has a population of about 2000 inhabitants. The size of the island satisfies the main requirement for negligible local aerosol emissions (cars are not allowed in the island). Apart from sea spray particles, that constitute the background aerosol component around the island, the only case of regional pollution influence is under northerly winds when the island is within the outflow of pollution from Athens. In the case of winds from southerly directions, most of the Athenian sources of aerosols do not reach Hydra island.

For the design of the experiment, paintings and measurements during relatively low and high AOD cases was the main goal. According to Gerasopoulos et al. (2011),

Table 1. Correlation coefficients between volcanic aerosol indices and AOD proxies shown in Fig. 4.

1500–2000	DVI	AOD (this study)	AOD (Robertson)	AOD (Crowley and Unterman)	AOD (Sato)	AOD (Stothers)	Sulfate (Gao)
DVI	1						
AOD (this study)	**0.85** [102]	1					
AOD (Robertson)	**0.65** [227]	**0.58** [118]	1				
AOD (Crowley and Unterman)	**0.57** [154]	**0.54** [74]	**0.80** [239]	1			
AOD (Sato)	**0.65** [66]	**0.55** [61]	**0.57** [126]	**0.91** [78]	1		
AOD (Stothers)	(*) [29]	(*) [21]	**0.83** [37]	(*) [29]	**0.92** [38]	1	
Sulfate (Gao)	(*) [23]	(*) [14]	**0.88** [33]	(*) [24]	(*) [11]	(*) [6]	1

Bold: all the above correlations are significant at the 99 % confidence level (t test).
* missing correlations are those possessing less than 30 years of data.
In brackets: number of pairs.

the typical background AOD for the area is 0.12–0.13 corresponding to long and fast trajectories from westerly to northerly directions, with origin from high altitudes over the Atlantic. Higher aerosol loading over the area is related to the advection of dust particles from desert and arid locations of North Africa and is in the AOD range of 0.3–0.4. The most frequent season for dust outbreaks over the eastern Mediterranean is well documented to be in late spring (e.g. Kalivitis et al., 2007; Gerasopoulos et al., 2011) and early summer (the latter mostly as elevated dust layers; Papayannis et al., 2008).

For the selection of the experiment days, a regional model designed to simulate and forecast the atmospheric cycle of mineral dust aerosol over the campaign site was deployed. In particular, forecasts from the BSC-DREAM8b dust regional model were used (Nickovic et al., 2001) and the period finally selected to combine an AOD episode followed by clean conditions and the painter's availability was 19–20 June 2010.

The instrumentation used for the campaign, included a multi-filter rotating shadowband radiometer (MFR-7 Yankee Env. System Inc., Turner Falls, MA) and a Microtops II sunphotometer (Solar Light Inc., Philadelphia, USA). The MFR-7 installed at Hydra was used to perform measurements of the total and diffuse solar irradiance to calculate the direct component of the irradiance (Harrison et al., 1994). MFR-7 provided 1 min average measurements and from these the AOD values at 500 nm was extracted. The instrument performs valid measurements during daytime and under clear sky conditions. The methodology followed for the extraction of the AOD values from direct solar irradiance is thoroughly described in Gerasopoulos et al. (2003). The calibrated handheld sunphotometer (Microtops II) was used to provide the AOD at 1020 nm, at 10 min intervals.

5.2 Experimental Results and discussion

As mentioned, the experiment took place in Hydra on 19 and 20 June 2010. During the campaign, a Saharan dust event passed over Greece (18–21 June 2010). On these two dates master Tetsis created two successive paintings; before and during sunset on the 19 and two additional paintings at sunset on the next day, 20 June 2010. Although the typical size and vertical profile of the Saharan aerosols differ from the volcanic ones, their effect on solar irradiance and R / G close to sunset was proved to be significant because of their relative high values of AOD (~ 0.25 at 500 nm). The Tetsis experiment has initially started as an experiment dedicated to investigate if AOD's can be calculated from such a live study. During the two day experiment the substantial difference between the aerosol condition of the first and the second day provided a more adequate data set, supporting the assumption that a painter is able to reproduce such an aerosol change. Quantitatively it has been proven that this assumption was correct, as analysed in the following. In the next paragraph it will be shown that the Saharan dust outbreak of the 19 June has been found to affect the R / G ratios of Tetsis' paintings.

The results from the BSC-DREAM8b model simulations of the space and time evolution of the columnar dust loading for the campaign days (19 and 20 June,) are shown in Fig. 6, as isopleths of AODs. Additionally, the wind fields at 3000 m heights are superimposed, showing clearly a southwestern flow affecting the site in both campaign days. No precipitation or cloudiness prevailed over Greece during the campaign period (Fig. 6 – upper panel), also corroborated by MODIS satellite images (not shown here). A massive transport of dust from the Saharan desert was observed on the 19 June over Greece and western Turkey, while on 20 June the centre of the dust plume moved to the east and spread and declined (Fig. 6 – lower panel). Following the BSC-DREAM8b simulations, the dust load reached maximum columnar concentration values of the order of $0.75\,\mathrm{g\,m^{-2}}$ over the Hydra site on the 19 June.

The model simulations agree with real-time measurements, as shown in Fig. 7 by the time evolution of the observed AOD values on site for 19 and 20 June, measured with MFR-7 and Microtops. As stated before, the local pollution

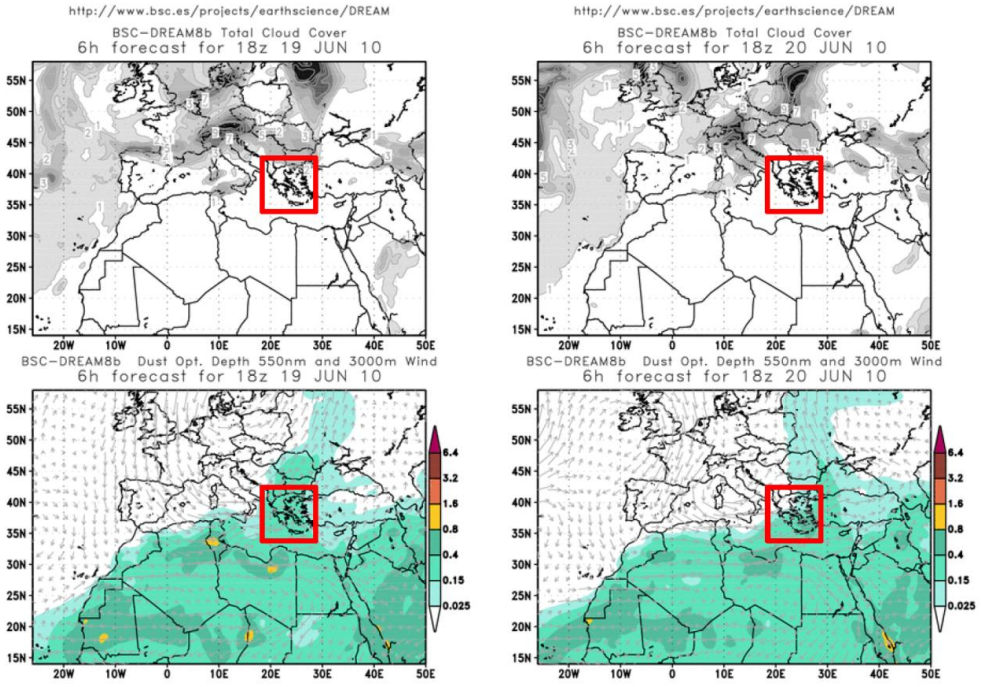

Fig. 6. Dust optical (AOD) depth at 550 nm and 3000 m wind fields over Greece for the 19 and 20 June 2010, as simulated by the BSC/DREAM model (18:00 UTC). The greater area of Greece is indicated by a red-lined rectangle. The island of Hydra is on the centre of this shape.

at Hydra is considered negligible and under southerly flows urban pollution from Athens does not reach the island. The meteorological conditions prevailing during both days (at sunset hours) were similar, namely temperatures between 28 and 30 °C (slightly higher on the second day) relative humidity between about 45 and 60 %, and calm wind conditions (1–2 m s^{-1}). The AOD values observed at Hydra, for the most part, can be attributed to the presence of the Saharan dust aerosol and follow the temporal evolution depicted by the dust simulations shown in Fig. 6, from which we see higher AOD values on 19 June and lower on the next day at Hydra. The temporal decay is profound also in the Microtops measurements at 1020 nm, performed at Hydra and shown also in Fig. 7.

Sunphotometric measurements are a trustworthy source for identifying the Saharan dust presence, for which we expect higher AOD values and lower spectral dependences between the multi-wavelength AOD retrievals. This is clearly seen in the data presented in Fig. 7, where higher AODs for 19 June are accompanied by lower spectral dependences between the 500 and 1020 nm channels. Moreover, the respective Ångström exponents were on average 0.4 on the first day, indicative of coarse dust aerosols and in the range 0.7–1.0 on the second day, representing a mixture of sea salt particles with low loadings of continental aerosols (see Gerasopoulos et al., 2011, for indicative ranges of Ångström exponents in the area).

Acknowledging the good performance of the BSC-DREAM8b model for the days of our campaign, we present in Fig. 8 the simulations of the vertical distribution of Saharan dust concentrations over the area for 19 and 20 June 2010. As can be seen from that Figure, large dust concentrations in the lowest one kilometre were observed on the 19 of June, while on the next day the dust concentrations declined significantly, in the boundary layer and in the column as well. We focus mainly on the aerosol load in the planetary boundary layer since this is expected to impact mostly the painter's perception during the late afternoon hours. It is evident that the dust concentrations within the first kilometre are four (4) times higher on 19 June than those simulated on 20 June.

Figure 9 shows the temporal evolution of the MFR-7 AOD values at 550 nm during the two days of the campaign together with the R / G ratios from a digital camera on site and from the high precision digital images (produced by National Gallery, London, with the methodology described in paragraph 2) of Tetsis paintings (Fig. 10) for the two sunset cases (high aerosol and low aerosol over Hydra). The paintings were transported to the National Gallery where the digital protocol analysis was done. On 19 June 2010 (Fig. 9, upper panel), the estimated AOD differences between the paintings and the closest time digital photos is ±0.02. However, a bias of about 30 % is revealed between these and the MFR measurements on the day of the Saharan dust event. In all three types of measurements/estimations, the variability of AOD

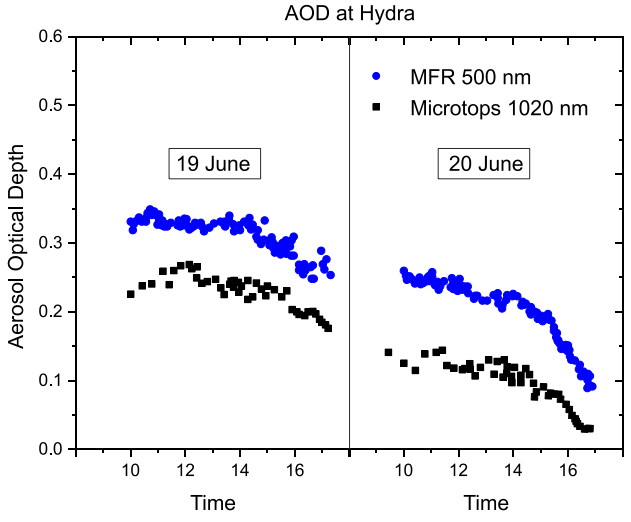

Fig. 7. MFR-7 AOD retrievals at 500 nm on 19 and 20 June 2010 at Hydra campaign site. Microtops II AOD retrievals at 1020 nm are superimposed.

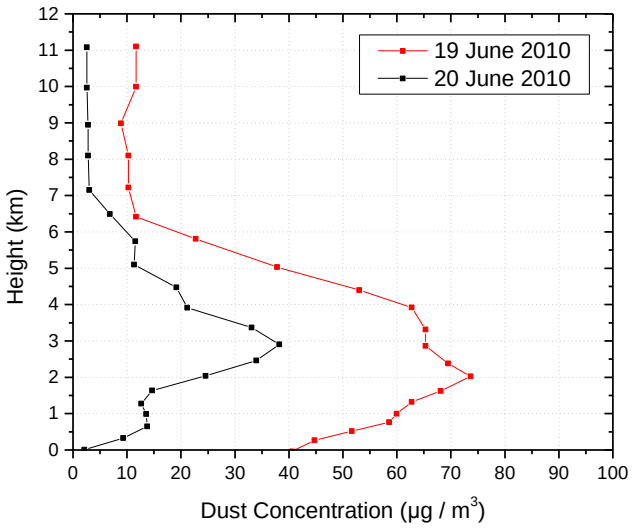

Fig. 8. Vertical distribution of the Saharan dust concentration loading ($\mu g\,m^{-3}$) for the 19 and 20 June 2010, as simulated by the BSC/DREAM model (18:00 UTC).

with time shows a negative trend as we move from 19 June to the evening of 20 June. On 20 June 2010, the agreement between the digitally derived and the measured AOD values is substantially improved: differences as small as 0.02 can be found. The measured decrease of the AOD values is also successfully represented by the digital estimations. Under each painting a digital photograph at the centre of the time interval it took to paint each painting is displayed for comparison.

Finally, a comparison between the impact of mineral aerosol (Saharan dust) and the impact of a typical volcanic aerosol in terms of RGB is also attempted. The mineral aerosol during the Hydra experiment at 500 nm was measured to vary close to 0.25. Therefore, we have made model runs with the volcanic aerosol setting the volcanic AOD case at 500 nm also equal to 0.25. Note here that the mean volcanic AOD (500 nm) in our paintings is very close to that number and is equal to 0.22. Figure 11 shows the percent difference in R / G ratios between the ones measured in the Hydra Saharan dust aerosol profile and a typical modelled volcanic aerosol profile as was used previously in this work. In both cases AOD (500 nm) was set to 0.25. The ratios are shown as isopleths in a graph where the position of the sun is fixed at 80° solar zenith angle. It was quite surprising to see that although both the nature, size and the vertical profiles of the Saharan and the volcanic aerosols differ, their effect on R / G overhead ratios in the sky induce so small a difference ranging from a minimum of −2.6 % to a maximum +1.6 %, depending on the solar zenith angle and the angle relative to the position of the sun.

6 Conclusions

Understanding the atmospheric composition of the past centuries is a very difficult task due to scarcity of available measurements. Especially for atmospheric components such as aerosols and their variability over the past 500 years, relevant information is rare (Thornes and Constable, 1999; Grattan, 2006; Zerefos et al., 2007). In this work we have expanded the idea of Zerefos et al. (2007), which used an alternative and indirect way of using the Ångström's law of atmospheric physics that describes the different effects of aerosols on the different wavelengths (colours) of solar light, together with the use of an alternative "database of solar light representations", calculated from paintings by great masters in the past centuries.

At first, a series of paintings by master painters (in the period of 1500–2000) have been revisited and comparisons between digital images of paintings from lower resolution vs. high resolution, derived from high precision protocols, showed similar results, as far as the R / G ratios measured at sunsets are concerned. Statistically significant correlation coefficients were found between the R / G ratio values retrieved from low quality/resolution and high quality/resolution digital images at a sample of 124 landscape paintings from the Tate Gallery. The earlier estimates of the aerosol optical depth at 550 nm (based on R / G calibrated ratios from paintings) and the radiative transfer model by Mayer and Kylling (2005) and Mayer and Emde (2007) were used to compile an independent time series with AODs during 1500–2000. The correlation coefficients between other proxy indices and the estimated AODs from the R / G ratios from paintings are statistically significant. Also the precision by which the extreme

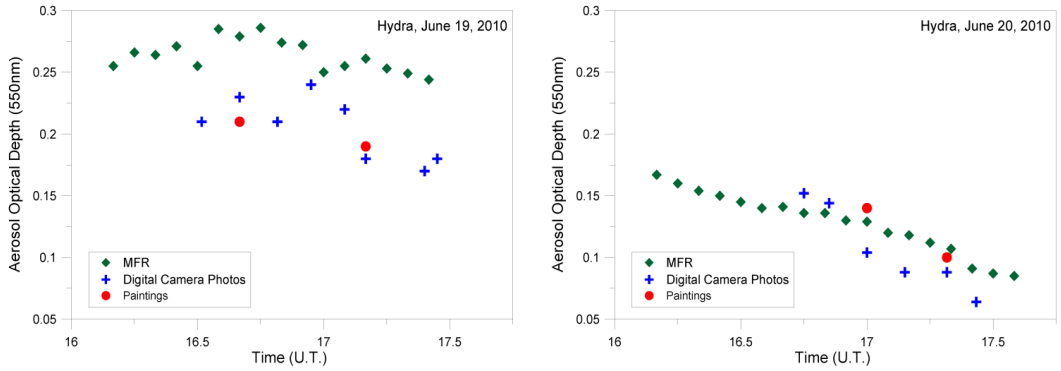

Fig. 9. The AOD values from the MFR measurements, the estimations from the digital images and the calculations from R / G ratios of the Hydra sunset paintings for 19 June (left panel, higher aerosol content) and on the 20 June 2010 (right panel, lower aerosol content).

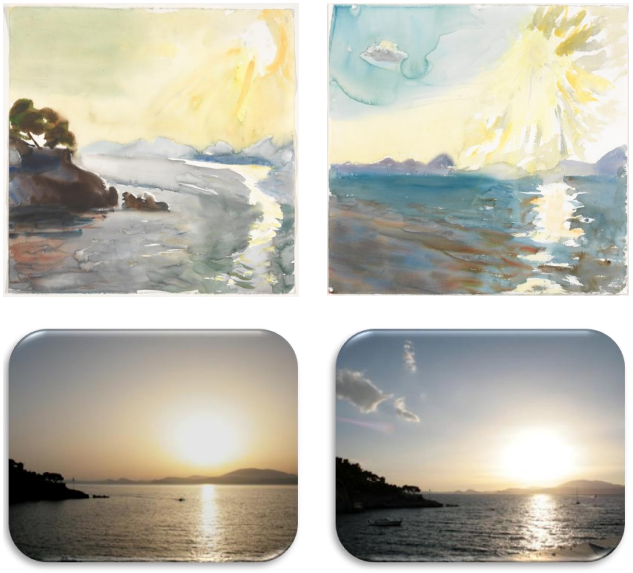

Fig. 10. Upper: digitally compressed paintings by P. Tetsis at the Hydra experiment under higher (left panel) and lower (right panel) AOD conditions. Bottom: digital camera photos of the landscape. Under each painting a digital photograph at the centre of the time interval it took to paint each painting is displayed for comparison (see text).

AODs between paintings and proxies, during large volcanic eruptions, match in most cases.

The comparison between 50-year averages of the AODs (from R / G paintings) with the total sulfate in ice core and the stratospheric AOD, from which the year of known large volcanic eruptions and the three years that followed were excluded, shows that compared to the pre-industrial period, the industrial period had higher aerosol content, as it is well known and expected from independent data sets in the literature (e.g. Neftel et al., 1985; Robock and Free, 1995; Robertson et al., 2001; Forster et al., 2007). Based on the information retrieved from the paintings studied, we estimated this increase to range from 0.15 (middle 19th century) to about 0.20 (by the end of the 20th century).

Finally, to corroborate our findings, an experiment was designed in which a master painter/colourist painted successive sunsets during the passage of a Saharan dust outbreak over our experimental site (island of Hydra, Greece) on 19 and 20 June 2010. The master painter did not know anything about the passage of a Saharan dust event. Our independent sun-photometric measurements at Hydra confirmed that the calculated AOD values from R / G ratios measured in the master colourist paintings, matched quite well to the AOD values measured in situ as well as with measurements from a digital camera. It should be noted here that all four watercolours by Panayiotis Tetsis were digitized using the same procedures and standards applied to all works of art photographed by the Photographic Department of the National Gallery, London. These findings point to the conclusion that the experiment provides a new presentation of how a painter, a digital camera and scientific instruments capture changes in R / G ratios at high and low aerosol overhead cases.

The new information in the paper can be summarized as follows:

The comparison of high precision with low precision colour protocol images at independent samples of paintings from the Tate and the National Galleries in London strengthen the tentative results proposed in an earlier paper by Zerefos et al. (2007).

AODs from a multi-hundred sample of paintings show statistically significant correlations with independent proxies.

Structural differences in paintings do not seem to alter the above results. The signal-to-noise ratios following volcanic eruptions are statistically significant.

When averaged in 50-year intervals, AODs from paintings in non-volcanic years agree with completely independent data sets with the observed increases of the industrial aerosol in the past 150 years.

R / G ratios calculated from different natural profiles such as from volcanic aerosols and Saharan mineral aerosols show

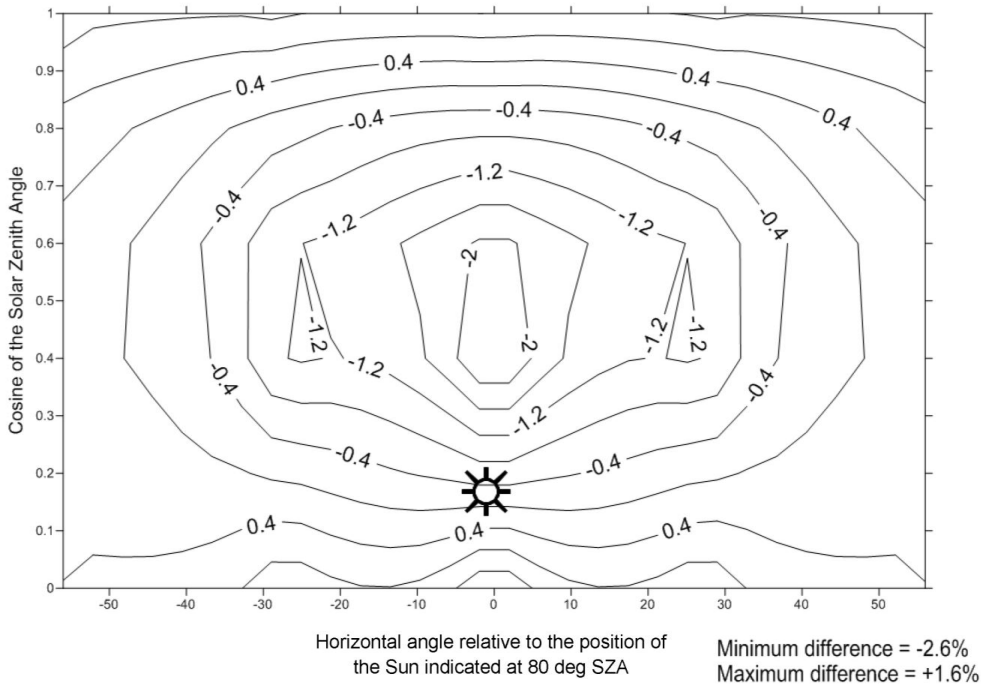

Fig. 11. Percent difference in R / G ratios between the measured at Hydra Sahara dust mineral aerosol profile and a typical modelled volcanic aerosol profile. In both cases AOD (500 nm) was set to 0.25.

very small differences. This explains how the experiment performed with an internationally known master colourist arrived at similar results with an increase in R / G ratios during the passage of a Saharan dust event.

Regardless of the school, red-to-green ratios from great masters can provide independent proxy AODs that correlate with widely accepted proxies and with independent measurements.

The main conclusion of the paper is that nature speaks to the hearts and souls of the artists. When colouring sunsets the R / G ratios perceived by the brain contain important environmental information. It remains to an interdisciplinary community to study further the evidence presented in this research.

Acknowledgements. The LibRadtran team (www.libradtran.org) is acknowledged for providing the model algorithm. The National Gallery is acknowledged for providing 186 landscape paintings of high quality analysis at no charge. BSC-DREAM8b Saharan dust simulations were kindly provided by the Barcelona Supercomputing Centre. The set of high resolution 124 paintings from Tate were purchased at cost and the four watercolour paintings by Panayiotis Tetsis were photographed using the same procedures and standards applied to all works of art photographed by the Photographic Department of the National Gallery, London. We greatly acknowledge the support provided by the Mariolopoulos-Kanaginis Foundation for the Environmental Sciences and the European Union's 7th Framework Programme (FP7/2007-2013) under grant agreement no. 218793 (project title: Monitoring Atmospheric Composition and Climate). The authors would like to thank Alan Robock and two anonymous reviewers for their valuable comments.

Edited by: N. Mihalopoulos

References

Ammann, C. and Naveau, P.: Statistical analysis of tropical explosive volcanism occurences over the last 6 centuries, Geophy. Res. Lett., 30, 1210, doi:10.1029/2002GL016388, 2003.

Crowley, T. J. and Unterman, M. B.: Technical details concerning development of a 1200 yr proxy index for global volcanism, Earth Syst. Sci. Data, 5, 187–197, doi:10.5194/essd-5-187-2013, 2013.

Forster, P., Ramaswamy, V., Artaxo, P., Berntsen, T., Betts, R., Fahey, D. W., Haywood, J., Lean, J., Lowe, D. C., Myhre, G., Nganga, J., Prinn, R., Raga, G., Schulz M., and Van Dorland, R.: Changes in Atmospheric Constituents and in Radiative Forcing, in: Climate Change 2007: The Physical Science Basis, Contribution of Working Group I to the Fourth Assessment, Report of the Intergovernmental Panel on Climate Change, edited by: Solomon, S., Qin, D., Manning, M., Chen, Z., Marquis, M., Averyt, K. B., Tignor, M., and Miller, H. L., Cambridge University Press, Cambridge, UK, New York, NY, USA, 996 pp., 2007.

Gao, C., Robock, A., and Ammann, C.: Volcanic forcing of climate over the past 1500 years: An improved ice-core-based index for climate models, J. Geophys. Res., 113, D23111, doi:10.1029/2008JD010239, 2008.

Gerasopoulos, E., Andreae, M. O., Zerefos, C. S., Andreae, T. W., Balis, D., Formenti, P., Merlet, P., Amiridis, V., and

Papastefanou, C.: Climatological aspects of aerosol optical properties in Northern Greece, Atmos. Chem. Phys., 3, 2025–2041, doi:10.5194/acp-3-2025-2003, 2003.

Gerasopoulos, E., Amiridis, V., Kazadzis, S., Kokkalis, P., Eleftheratos, K., Andreae, M. O., Andreae, T. W., El-Askary, H., and Zerefos, C. S.: Three-year ground based measurements of aerosol optical depth over the Eastern Mediterranean: the urban environment of Athens, Atmos. Chem. Phys., 11, 2145–2159, doi:10.5194/acp-11-2145-2011, 2011.

Grattan, J.: Aspects of Armageddon: an exploration of the role of volcanic eruptions in human history and civilization, Quartern. Int., 151, 10–18, 2006.

Harrison, L., Michalsky, J., and Berndt, J.: Automated multifilter rotating shadow-band radiometer: an instrument for optical depth and radiation measurements, Appl. Optics, 33, 5118–5125, 1994.

Kalivitis, N., Gerasopoulos, E., Vrekoussis, M., Kouvarakis, G., Kubilay, N., Hatzianastassiou, N., Vardavas, I., and Mihalopoulos, N.: Dust transport over the Eastern Mediterranean from TOMS, AERONET and surface measurements, J. Geophys. Res., 112, D03202, doi:10.1029/2006JD007510, 2007.

Lamb, H. H.: Volcanic dust in the atmosphere, with a chronology and assessment of its meteorological significance, Philos. T. R. Soc. Lond., 266, 425–533, 1970.

Lamb, H. H.: Supplementary volcanic dust veil assessments, Climate Monitor, 6, 57–67, 1977.

Lamb, H. H.: Uptake of the chronology of assessments of the volcanic dust veil index, Climate Monitor., 12, 79–90, 1983.

Mayer, B. and Emde, C.: Comment on "Glory phenomenon informs of presence and phase state of liquid water in cold clouds" by Nevzorov, A. N., Atmos. Res., 84, 410–419, 2007.

Mayer, B. and Kylling, A.: Technical note: The libRadtran software package for radiative transfer calculations – description and examples of use, Atmos. Chem. Phys., 5, 1855–1877, doi:10.5194/acp-5-1855-2005, 2005.

McCamy, C. S., Marcus, H., and Davidson, J. G.: A color-rendition chart, J. Appl. Photogr. Eng., 2, 95–99, 1976.

Neftel, A., Beer, J., Oeschger, H., Zurcher, F., and Finkel, R. C.: Sulphate and nitrate concentrations in snow from South Greenland 1895–1978, Nature, 314, 611–613, doi:10.1038/314611a0, 1985.

Nickovic, S., Kallos, G., Papadopoulos, A., and Kakaliagou, O.: A model for prediction of desert dust cycle in the atmosphere, J. Geophys. Res., 106, 18113–18129, doi:10.1029/2000JD900794, 2001.

Papayannis, A., Amiridis, V., Mona, L., Tsaknakis, G., Balis, D., Bösenberg, J., Chaikovski, A., De Tomasi, F., Grigorov, I., Mattis, I., Mitev, V., Müller, D., Nickovic, S., Perez, C., Pietruczuk, A., Pisani, G., Ravetta, F., Rizi, V., Sicard, M., Trickl, T., Wiegner, M., Gerding, M., Mamouri, R. E., D'Amico, G., and Pappalardo, G.: Systematic lidar observations of Saharan dust over Europe in the frame of EARLINET (2000–2002), J. Geophys. Res., 113, D10204, doi:10.1029/2007JD009028, 2008.

Robertson, A., Overpeck, J., Rind, D., Mosley-Thompson, E., Zielinski, G., Lean, J., Koch, D., Penner, J., Tegen, I., and Healy, R.: Hypothesized climate forcing time series for the last 500 years, J. Geophys. Res., 106, 14783–14803, 2001.

Robock, A.: Volcanic eruptions and climate, Rev. Geophys., 38, 191–219, 2000.

Robock, A. and Free, M. P.: Ice cores as an index of global volcanism from 1850 to the present, J. Geophys. Res., 100, 11549–11567, 1995.

Sato, M., Hansen, J. E., McCormick, M. P., and Pollack, J. B.: Stratospheric aerosol optical depths 1850–1990, J. Geophys. Res., 98, 22987–22994, 1993.

Saunders, D., Cupitt, J., White, C., and Holt, S.: The MARC II Camera and the scanning initiative at the national gallery, National Gallery Technical Bulletin, 23, 76–82, 2002.

Stothers, R. B.: Major optical depth perturbations to the stratosphere from volcanic eruptions: pyrheliometric period 1881–1960, J. Geophys. Res., 101, 3901–3920, 1996.

Stothers, R. B.: Major optical depth perturbations to the stratosphere from volcanic eruptions: Stellar extinction period 1961–1978, J. Geophys. Res., 106, 2993–3003, 2001.

Thornes, J. E. and Constable, J.: John Constable's skies: A Fusion of Art and Science, Ed. Continuum, 288 pp., 1999.

Wild, M.: Enlightening Global Dimming and Brightening, B. Am. Meteorol. Soc., 93, 27–37, 2012.

Zerefos, C. S., Gerogiannis, V. T., Balis, D., Zerefos, S. C., and Kazantzidis, A.: Atmospheric effects of volcanic eruptions as seen by famous artists and depicted in their paintings, Atmos. Chem. Phys., 7, 4027–4042, doi:10.5194/acp-7-4027-2007, 2007.

Zielinski, G. A.: Stratospheric loading and optical depth estimates of explosive volcanism over the last 2100 years derived from the Greenland Ice Sheet Project 2 ice core, J. Geophys. Res., 100, 20937–20955, 1995.

Zielinski, G. A., Mayewski, P. A., Meeker, L. D., Whitlow, S., and Twickler, M. S.: A 110,000-yr record of explosive volcanism from the GISP2 (Greenland) ice core, Quaternary Res., 45, 109–188, 1996.

Appendix A

Table A1. Paintings from the Tate Gallery analysed in this work.

Image ID	Artist name	Title
1. D00670	Turner, Joseph Mallord William	Windmill on Hill: Valley and Winding River in Middle Distance; Sunset Effect
2. D02474	Turner, Joseph Mallord William	Helmsley Sketchbook [Finberg LIII], Distant View of Whitby from the Moors: A Windmill against a
3. D04118	Turner, Joseph Mallord William	Studies for Pictures Sketchbook [Finberg LXIX], Study for the Composition of "Dolbadern Castle"
4. D04119	Turner, Joseph Mallord William	Studies for Pictures Sketchbook [Finberg LXIX], Study for the Composition of "Dolbadern Castle",
5. D04127	Turner, Joseph Mallord William	Studies for Pictures Sketchbook [Finberg LXIX], Snowy Hills beside a Lake: Evening Sky
6. D04128	Turner, Joseph Mallord William	Studies for Pictures Sketchbook [Finberg LXIX], Study for the Composition of "Dolbadern Castle",
7. D08176	Turner, Joseph Mallord William	Moonlight at Sea (The Needles)
8. D12502	Turner, Joseph Mallord William	Skies Sketchbook [Finberg CLVIII], Red Sky and Crescent Moon
9. D16131	Turner, Joseph Mallord William	Naples: Rome. C. Studies Sketchbook [Finberg CLXXXVII], The Roman Campagna from Monte Testaccio
10. D16482	Turner, Joseph Mallord William	Small Roman Colour Studies Sketchbook [Finberg CXC], Moonlight over the Campagna
11. D20254	Turner, Joseph Mallord William	Mayen in the Eifel
12. D22663	Turner, Joseph Mallord William	Evening: A Windmill at Sunset
13. D22664	Turner, Joseph Mallord William	Sunset across the Park from the Terrace of Petworth House
14. D22666	Turner, Joseph Mallord William	Evening: A Boat on a River with a Distant Tower
15. D22674	Turner, Joseph Mallord William	Sunset over the Ridge Seen from the North Pond in Petworth Park
16. D22716	Turner, Joseph Mallord William	Setting Sun
17. D22719	Turner, Joseph Mallord William	The Setting Sun over Petworth Park
18. D22767	Turner, Joseph Mallord William	Petworth Park: Sunset ("Glade and Greensward")
19. D22768	Turner, Joseph Mallord William	Sunset: A Boat on a River
20. D24635	Turner, Joseph Mallord William	A Distant View of the Upperton Monument, from the Lake in Petworth Park
21. D24640	Turner, Joseph Mallord William	Harbour Scene at Sunrise, possibly Margate
22. D24666	Turner, Joseph Mallord William	The Scarlet Sunset
23. D24698	Turner, Joseph Mallord William	Turner's Annual Tour: The Seine 1834 Watercolours, Le Havre: Sunset in the Port
24. D24757	Turner, Joseph Mallord William	A View of Metz from the North
25. D25132	Turner, Joseph Mallord William	Sunlight over Water
26. D25141	Turner, Joseph Mallord William	Cilgerran Castle, Pembrokeshire
27. D25144	Turner, Joseph Mallord William	The River: Sunset
28. D25201	Turner, Joseph Mallord William	Looking out to Sea
29. D25233	Turner, Joseph Mallord William	River with Trees: Sunset
30. D25246	Turner, Joseph Mallord William	Castle Upnor, Kent: Preparatory Study
31. D25249	Turner, Joseph Mallord William	River: Sunset
32. D25253	Turner, Joseph Mallord William	Studies of Skies
33. D25258	Turner, Joseph Mallord William	Evening
34. D25263	Turner, Joseph Mallord William	The Line of Cliffs
35. D25300	Turner, Joseph Mallord William	The Castle by the Sea
36. D25303	Turner, Joseph Mallord William	River Scene: Sunset
37. D25315	Turner, Joseph Mallord William	Sunset
38. D25329	Turner, Joseph Mallord William	Sunset
39. D25330	Turner, Joseph Mallord William	Fiery Sunset
40. D25331	Turner, Joseph Mallord William	Crimson Sunset
41. D25332	Turner, Joseph Mallord William	Sunset over Water
42. D25336	Turner, Joseph Mallord William	A Ruin: Sunset
43. D25338	Turner, Joseph Mallord William	Twilight over the Waters
44. D25361	Turner, Joseph Mallord William	A Stormy Sunset
45. D25368	Turner, Joseph Mallord William	Sequels to the Liber Studiorum ("Little Liber") Watercolours, The Distant Tower: Evening
46. D25403	Turner, Joseph Mallord William	The Yellow Sky
47. D25412	Turner, Joseph Mallord William	A Pink Sky above a Grey Sea
48. D25430	Turner, Joseph Mallord William	Sequels to the Liber Studiorum ("Little Liber") Watercolours, Gloucester Cathedral
49. D25433	Turner, Joseph Mallord William	Running Wave in a Cross-Tide: Evening

Table A1. Continued.

Image ID	Artist Name	Title
50. D25443	Turner, Joseph Mallord William	Barnstaple Bridge at Sunset
51. D25446	Turner, Joseph Mallord William	Study for "The Golden Bough"
52. D25450	Turner, Joseph Mallord William	Sunset
53. D25474	Turner, Joseph Mallord William	Rochester Castle and Bridge
54. D25507	Turner, Joseph Mallord William	Sunset over the Sea
55. D25514	Turner, Joseph Mallord William	St Michael's Mount from Marazion, Cornwall
56. D27601	Turner, Joseph Mallord William	Sunset over a City
57. D27689	Turner, Joseph Mallord William	Rogers's Poems 1835 Watercolours, Tornaro (Rogers's "Poems")
58. D27716	Turner, Joseph Mallord William	Rogers's Poems 1835 Watercolours, Datur Hora Quieti
59. D28994	Turner, Joseph Mallord William	Sunset over Lake or River
60. D29026	Turner, Joseph Mallord William	Sunset
61. D32130	Turner, Joseph Mallord William	Roll Sketchbook of Venice [Finberg CCCXV], Venice: Sunset over Santa Maria della Salute and the
62. D32152	Turner, Joseph Mallord William	Venice: Sunset
63. D32185	Turner, Joseph Mallord William	View of Town, with Yellow Sky
64. D32191	Turner, Joseph Mallord William	Sunset on the Sea
65. D32203	Turner, Joseph Mallord William	Orange Sunset
66. D33479	Turner, Joseph Mallord William	Fribourg, Lausanne and Geneva Sketchbook [Finberg CCCXXXII], Geneva, the Jura Mountains and
67. D33484	Turner, Joseph Mallord William	Fribourg, Lausanne and Geneva Sketchbook [Finberg CCCXXXII], Sunset on a Lake
68. D33501	Turner, Joseph Mallord William	Fribourg, Lausanne and Geneva Sketchbook [Finberg CCCXXXII], Sunset, Lake of Lucerne
69. D33504	Turner, Joseph Mallord William	Fribourg, Lausanne and Geneva Sketchbook [Finberg CCCXXXII], Mont Pilatus: Sunset
70. D35260	Turner, Joseph Mallord William	The Whalers Sketchbook [Finberg CCCLIII], Sea Monsters and Vessels at Sunset
71. D35378	Turner, Joseph Mallord William	Ideas of Folkestone Sketchbook [Finberg CCCLVI], Sunset, over the Water
72. D35392	Turner, Joseph Mallord William	Ambleteuse and Wimereux Sketchbook [Finberg CCCLVII], Yellow Sun over Water
73. D35394	Turner, Joseph Mallord William	Ambleteuse and Wimereux Sketchbook [Finberg CCCLVII], Sunset at Ambleteuse
74. D35927	Turner, Joseph Mallord William	A Lurid Sunset
75. D35943	Turner, Joseph Mallord William	Sunset over Yellow-Green Waters
76. D35950	Turner, Joseph Mallord William	Yellow Sunset
77. D35973	Turner, Joseph Mallord William	The Bass Rock
78. D35986	Turner, Joseph Mallord William	Sunset: Study for "Flint Castle, on the Welsh Coast"
79. D36060	Turner, Joseph Mallord William	The Rigi
80. D36078	Turner, Joseph Mallord William	Sunset. (Sunrise)
81. D36123	Turner, Joseph Mallord William	The Red Rigi: Sample Study
82. D36149	Turner, Joseph Mallord William	Sunset, with Smoke from a Distant Steamer
83. D36153	Turner, Joseph Mallord William	Distant View of Regensburg from the Dreifaltigkeitsberg
84. D36159	Turner, Joseph Mallord William	Sunset: A Fish Market on the Beach
85. D36174	Turner, Joseph Mallord William	The Walhalla, near Regensburg on the Danube
86. D36211	Turner, Joseph Mallord William	Lausanne: Sunset
87. D36242	Turner, Joseph Mallord William	Geneva
88. D36293	Turner, Joseph Mallord William	Yellow and Blue Sunset over Water
89. D36679	Turner, Joseph Mallord William	Sunset Seen from a Beach with Breakwater
90. N00304	Wilson, Richard	Lake Avernus and the Island of Capri
91. N00309	Gainsborough, Thomas	Boy Driving Cows near a Pool
92. N00342	Callcott, Sir Augustus Wall	Dutch Landscape with Cattle
93. N00499	Turner, Joseph Mallord William	The Decline of the Carthaginian Empire ...
94. N00519	Turner, Joseph Mallord William	Regulus
95. N00559	Turner, Joseph Mallord William	Petworth Park: Tillington Church in the Distance
96. N00560	Turner, Joseph Mallord William	Chichester Canal
97. N00886	Reynolds, Sir Joshua	Admiral Viscount Keppel
98. N00926	Crome, John	A Windmill near Norwich
99. N01290	Wilson, Richard	Landscape with Bathers, Cattle and Ruin
100. N01656	McLachlan, Thomas Hope	Evening Quiet

Table A1. Continued.

Image ID	Artist name	Title
101. N01876	Turner, Joseph Mallord William	Sunset
102. N01902	Brett, John	The British Channel Seen from the Dorsetshire Cliffs
103. N02064	Turner, Joseph Mallord William	The Chain Pier, Brighton
104. N02065	Turner, Joseph Mallord William	A Ship Aground
105. N02066	Turner, Joseph Mallord William	The Arch of Constantine, Rome
106. N02067	Turner, Joseph Mallord William	Tivoli: Tobias and the Angel
107. N02645	Crome, John	Moonrise on the Yare (?)
108. N02647	Wilson, Richard	River View, on the Arno (?)
109. N02701	Turner, Joseph Mallord William	The Lake, Petworth, Sunset
110. N02990	Turner, Joseph Mallord William	Ariccia (?): Sunset
111. N03026	Turner, Joseph Mallord William	Classical Harbour Scene
112. N03382	Turner, Joseph Mallord William	Claudian Harbour Scene
113. N04665	Turner, Joseph Mallord William	Sun Setting over a Lake
114. N04937	Ward, James	L'Amour de Cheval
115. N05361	Crome, John	Yarmouth Harbour – Evening
116. N05486	Turner, Joseph Mallord William	Sunset From the Top of the Rigi
117. N05530	Turner, Joseph Mallord William	Seacoast with Ruin, probably the Bay of Baiae
118. N05853	Boitard, Louis Philippe	An Exact Representation of the Game of Cricket
119. T00921	De Loutherbourg, Philip James	Travellers Attacked by Banditti
120. T03163	Garstin, Norman	Haycocks and Sun
121. T03543	Anderton, Henry	Mountain Landscape with Dancing Shepherd
122. T03883	Turner, Joseph Mallord William	The Lake, Petworth: Sunset, Fighting Bucks
123. T03884	Turner, Joseph Mallord William	The Lake, Petworth: Sunset, a Stag Drinking
124. T03885	Turner, Joseph Mallord William	Chichester Canal

Appendix B

Table B1. Volcanic eruptions in 1500–2000 with volcanic explosivity index (VEI) of 4 or more.

No.	Year	Volcano	VEI*	Reference
1	1522	? Arenal, Costa Rica (C-14: 1525)	4	[1]
2	1568	? Billy Mitchell (C-14: 1580)	6	[1]
3	1586	Kelut, Java	5?	[1]
4	1595	Raung, Java	5?	[1]
5		Ruiz, Colombia	4	[1]
6	1600	Huynaputina, Peru	6?	[1]
7	?*1605	Momotombo, Nicaragua	4	[1]
8	1622	? Colima, Mexico	4	[1]
9	C-14: 1630	Raoul Island, Kermadec	4	[1]
10	1641	Parker, Indonesia	6	[1]
11	1660	? Teon, Banda	4?	[1]
12		? Guagua Pichinchia, Ecuador	4	[1]
13	1665	? Long Island, New Guinea (C-14: 1660)	6?	[1]
14	1674	Gamkonora, Indonesia	5?	[1]
15	1680	Tongkoko, Sulawesi	5?	[1]
16	1693	Serua, Banda	4?	[1]
17	?1721	Raoul Island, Kermadec (C-14: 1720)	4	[1]
18		Cerro Bravo, Colombia (T)	4	[1]
19	?1737	Fuego, Guatemala	4?	[1]
20	1744	Cotopaxi, Equador	4	[1]
21	1760	Michoacan, Mexico	4	[1]
22		Makian, Indonesia	4?	[1]
23	1783	Lakagigar, Iceland	4	[2]
24	1794	? San Martin, Mexico	4?	[1]
25	?1808	Unknown	?	[1]
26	1813	Soufriere St. Vincent, W-Indies	4	[1]
27		Awu, Indonesia	4?	[1]
28		Suwanose-Jima, Japan	4	[1]
29	1815	Tambora, Indonesia	7	[1, 2]
30	1823	Galunggung, Java	5	[1]
31	1831	Babuyan Claro, Philippines	4?	[1]
32	1835	Coseguina, Nicaragua	5	[1, 2]
33	1861	Makian, Indonesia	4?	[1]
34	1875	Askja, Iceland	5	[2]
35	1880	Fuego, Guatemala	4?	[1]
36	1883	Krakatau, Indonesia	6	[1, 2]
37	1886	Tarawera, New Zealand	5	[2]
38	1890	Colima, Mexico	4	[1]
39	1902	Pelee, W-Indies	4	[1]
40		Soufriere St. Vincent, W-Indies	4	[1]
41	1903	Santa Maria, Guatemala	6	[1, 2]
42	1907	Ksudach, Kamchatka, Russia	5	[2]
43	?1911	Lolobau, SW-Pacific	4	[1]
44		Taal, Philippines	4	[1]
45	1912	Katmai, Alaska	6	[2]
46	1953	Ambrym, Vanuatu	4+	[1]
47		Lamington, New Guinea	4	[1]
48		Bagana, SW-Pacific	4	[1]
49	1963	Agung, Indonesia	4	[1, 2]
50	1968	Fernandina, Galapagos	4	[1]
51	1974	Fuego, Guatemala	4	[1]
52	1980	St. Helens, United States	5	[2]
53	1982	El Chichon, Mexico	5	[1, 2]
54	1991	Pinatubo, Philippines	6	[1, 2]

[1]: after Ammann and Naveau (2003) at ftp://ftp.ncdc.noaa.gov/pub/data/paleo/climate_forcing/volcanic_aerosols/ammann2003_eruptions.pdf.
[2]: Robock (2000)
* It should be mentioned that VEI is not a good index of stratospheric sulfate loading, since it measures the explosivity of an eruption and not its stratospheric injection.

Appendix C

R / G ratios with and without structural differences after Tambora (1815) and Krakatau (1883)

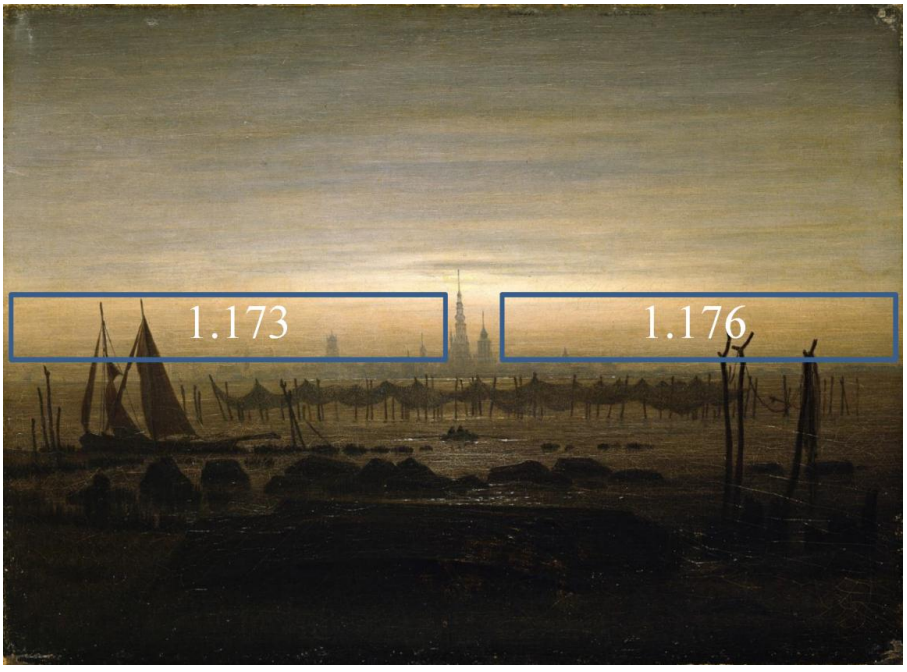

Fig. C1. Caspar David Friedrich, Griefswald in the Moonlight, 1817. Corresponding R / G ratios were averaged inside each box.

Fig. C2. Karl Friedrich Schinkel, The Banks of the Spree near Stralau, 1817. Corresponding R / G ratios were averaged inside each box.

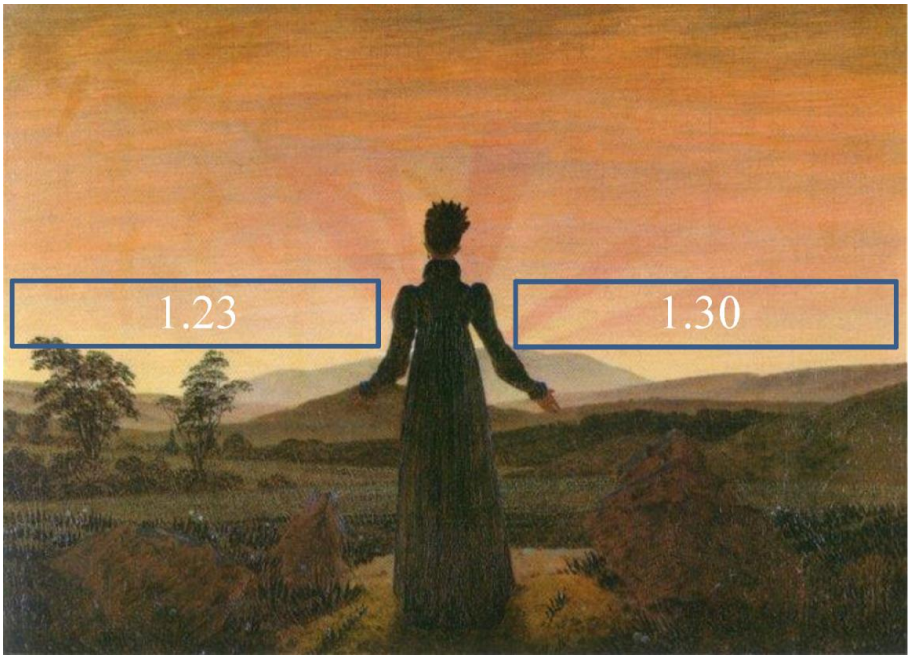

Fig. C3. Caspar David Friedrich, Woman in front of the Setting Sun, 1818. Corresponding R / G ratios were averaged inside each box.

Fig. C4. Joseph Mallord William Turner, Red sky and crescent moon, c. 1818. Corresponding R / G ratios were averaged inside the box.

Fig. C5. Edgar Degas, Landscape on the Orne, c. 1884. Corresponding R / G ratios were averaged inside each box.

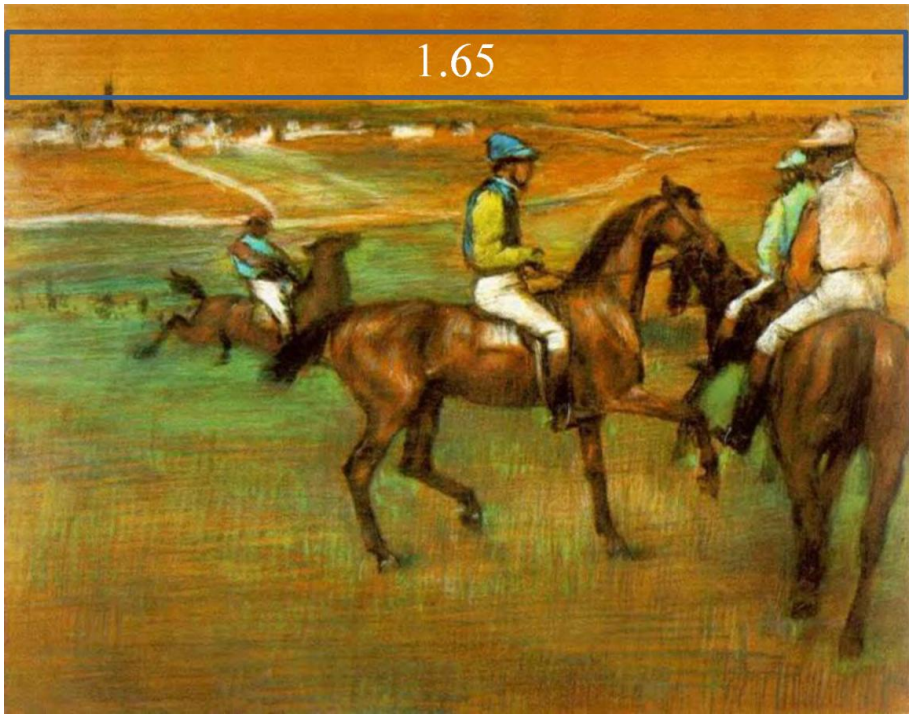

Fig. C6. Edgar Degas, Race Horses, 1885. Corresponding R / G ratios were averaged inside the box.

Appendix D

Table D1. Volcanic aerosol indices and AOD proxies shown in Fig. 4.

Year	N.H. DVI	N.H. AOD from paintings	AOD	AOD	AOD	AOD	Sulfate aerosols (Tg)
	(Lamb, 1970, 1977, 1983)	(this study)	(Robertson et al., 2001)	Crowley and Unterman (2013)	(Sato et al., 1993)	(Stothers, 1996, 2001)	(Gao et al., 2008)
1500	200	–	0.0010	–	–	–	–
1501	150	0.103	0.0117	–	–	–	–
1502	100	–	0.0110	–	–	–	–
1503	50	0.12	0.0110	0.01	–	–	1.72
1504	–	–	0.0002	0.003	–	–	–
1505	–	–	0.0076	0.008	–	–	–
1506	–	–	–	0.008	–	–	–
1507	–	–	–	0.002	–	–	–
1508	–	–	–	0.021	–	–	–
1509	–	–	0.0055	0.012	–	–	–
1510	–	–	0.0022	0.003	–	–	–
1511	–	–	0.0076	0.001	–	–	–
1512	–	–	–	–	–	–	4.24
1513	–	–	0.0112	–	–	–	–
1514	–	–	0.0008	–	–	–	–
1515	–	–	0.0037	0.016	–	–	–
1516	–	–	0.0000	0.005	–	–	–
1517	–	–	0.0010	0.001	–	–	–
1518	–	–	0.0007	–	–	–	–
1519	–	–	0.0007	–	–	–	–
1520	–	–	–	0.004	–	–	–
1521	–	–	0.0039	0.008	–	–	–
1522	–	–	0.0013	0.002	–	–	–
1523	–	–	0.0031	0.004	–	–	–
1524	–	–	0.0035	0.008	–	–	–
1525	–	–	0.0023	0.009	–	–	–
1526	–	–	0.0010	0.025	–	–	3.54
1527	–	–	0.0079	0.006	–	–	–
1528	–	–	–	0.003	–	–	–
1529	–	–	0.0068	–	–	–	–
1530	–	–	0.0026	0.003	–	–	–
1531	–	–	0.0025	0.001	–	–	–
1532	–	–	0.0007	–	–	–	–
1533	–	–	0.0041	0.002	–	–	–
1534	–	–	0.0002	–	–	–	3.86
1535	50	–	–	–	–	–	–
1536	50	–	0.0009	0.007	–	–	–
1537	50	–	0.0052	0.014	–	–	–
1538	–	–	0.0045	0.003	–	–	–
1539	–	–	0.0037	0.001	–	–	–
1540	–	–	0.0095	–	–	–	–
1541	–	–	0.0066	–	–	–	–
1542	–	–	0.0029	0.011	–	–	–
1543	–	–	0.0087	0.004	–	–	–
1544	–	–	0.0021	0.001	–	–	–
1545	–	–	–	–	–	–	–
1546	–	–	0.0023	–	–	–	–
1547	–	–	–	–	–	–	–

Table D1. Continued.

Year	N.H. DVI	N.H. AOD from paintings	AOD	AOD	AOD	AOD	Sulfate aerosols (Tg)
	(Lamb, 1970, 1977, 1983)	(this study)	(Robertson et al., 2001)	Crowley and Unterman (2013)	(Sato et al., 1993)	(Stothers, 1996, 2001)	(Gao et al., 2008)
1548	–	–	–	–	–	–	–
1549	–	–	0.0020	–	–	–	–
1550	–	–	0.0086	–	–	–	–
1551	–	–	0.0016	–	–	–	–
1552	–	–	0.0030	–	–	–	–
1553	100	–	0.0018	0.012	–	–	–
1554	500	–	0.0020	0.028	–	–	–
1555	350	–	0.0121	0.012	–	–	–
1556	200	–	0.0028	0.003	–	–	–
1557	100	0.168	–	–	–	–	–
1558	–	–	0.0007	–	–	–	–
1559	–	–	0.0018	–	–	–	–
1560	–	–	0.0006	–	–	–	–
1561	–	–	0.0003	0.03	–	–	–
1562	–	–	0.0037	0.01	–	–	–
1563	–	–	0.0028	0.019	–	–	–
1564	–	–	0.0039	0.006	–	–	–
1565	–	–	0.0168	0.001	–	–	–
1566	–	–	0.0011	–	–	–	–
1567	–	–	0.0004	0.012	–	–	–
1568	–	–	0.0033	0.007	–	–	–
1569	–	–	0.0007	0.002	–	–	–
1570	–	–	0.0041	0.011	–	–	–
1571	–	–	0.0151	0.015	–	–	–
1572	–	–	–	0.009	–	–	–
1573	–	–	0.0003	0.015	–	–	–
1574	–	–	0.0024	0.003	–	–	–
1575	–	–	0.0092	0.023	–	–	–
1576	–	–	0.0335	0.053	–	–	–
1577	–	–	0.0917	0.019	–	–	–
1578	–	–	0.0067	0.02	–	–	–
1579	–	–	0.0064	0.007	–	–	–
1580	–	–	0.0071	0.012	–	–	–
1581	–	–	0.0052	0.003	–	–	–
1582	–	–	0.0003	0.001	–	–	–
1583	–	–	–	0.011	–	–	–
1584	–	–	0.0068	0.003	–	–	24.23
1585	–	–	0.0018	0.053	–	–	–
1586	200	–	0.0868	0.018	–	–	–
1587	150	–	0.0639	0.004	–	–	–
1588	100	–	0.0143	0.015	–	–	–
1589	50	–	0.0059	0.005	–	–	–
1590	–	–	0.0029	0.001	–	–	–
1591	–	–	–	0.01	–	–	–
1592	–	–	–	0.003	–	–	–
1593	200	–	0.0421	0.019	–	–	9.54
1594	150	–	0.0620	0.068	–	–	–
1595	100	–	0.0101	0.028	–	–	–
1596	50	–	0.0010	0.021	–	–	–
1597	40	–	0.0008	0.007	–	–	–
1598	30	–	0.0016	0.001	–	–	–
1599	20	–	0.0147	–	–	–	–

Table D1. Continued.

Year	N.H. DVI	N.H. AOD from paintings	AOD	AOD	AOD	AOD	Sulfate aerosols (Tg)
	(Lamb, 1970, 1977, 1983)	(this study)	(Robertson et al., 2001)	Crowley and Unterman (2013)	(Sato et al., 1993)	(Stothers, 1996, 2001)	(Gao et al., 2008)
1600	10	0.084	0.0729	0.147	–	–	56.59
1601	400	–	0.0994	0.132	–	–	–
1602	300	–	0.0065	0.05	–	–	–
1603	210	–	0.0064	0.019	–	–	–
1604	110	–	0.0062	0.007	–	–	–
1605	10	–	0.0049	–	–	–	–
1606	20	–	0.0007	–	–	–	–
1607	50	0.112	0.0017	0.013	–	–	–
1608	50	–	0.0011	0.004	–	–	–
1609	50	–	0.0014	0.001	–	–	–
1610	40	0.097	0.0005	0.006	–	–	–
1611	30	–	–	0.002	–	–	–
1612	20	0.101	0.0018	–	–	–	–
1613	10	–	0.0059	0.005	–	–	–
1614	200	–	0.0010	0.014	–	–	–
1615	150	–	–	0.004	–	–	–
1616	100	–	–	0.001	–	–	–
1617	50	–	0.0003	–	–	–	–
1618	–	–	0.0072	–	–	–	–
1619	–	–	0.0209	–	–	–	5.23
1620	–	–	0.0042	–	–	–	–
1621	–	–	0.0017	0.025	–	–	–
1622	–	–	0.0102	0.033	–	–	–
1623	–	–	0.0017	0.007	–	–	–
1624	–	–	0.0056	0.002	–	–	–
1625	100	0.13	0.0069	–	–	–	–
1626	75	–	–	0.004	–	–	–
1627	50	0.115	0.0005	0.001	–	–	–
1628	25	–	0.0006	–	–	–	–
1629	–	–	0.0076	–	–	–	–
1630	–	–	0.0022	0.01	–	–	–
1631	120	–	–	0.003	–	–	–
1632	90	–	0.0022	0.001	–	–	–
1633	60	–	0.0010	–	–	–	–
1634	30	–	0.0030	–	–	–	–
1635	–	–	0.0053	–	–	–	–
1636	40	0.102	0.0048	–	–	–	–
1637	30	0.067	0.0014	–	–	–	–
1638	120	0.151	0.0004	–	–	–	–
1639	85	–	–	–	–	–	–
1640	150	0.284	0.0462	0.022	–	–	–
1641	400	–	0.0705	0.157	–	–	51.6
1642	275	0.35	0.0355	0.101	–	–	–
1643	175	0.125	0.0019	0.036	–	–	–
1644	75	–	–	0.013	–	–	–
1645	–	–	0.0036	0.027	–	–	–
1646	60	–	0.0089	0.007	–	–	–
1647	45	–	–	0.002	–	–	–
1648	30	0.097	0.0021	–	–	–	–
1649	15	0.08	–	–	–	–	–
1650	100	0.251	0.0017	–	–	–	–
1651	75	–	0.0015	–	–	–	–
1652	50	0.104	0.0010	–	–	–	–

Table D1. Continued.

Year	N.H. DVI	N.H. AOD from paintings	AOD	AOD	AOD	AOD	Sulfate aerosols (Tg)
	(Lamb, 1970, 1977, 1983)	(this study)	(Robertson et al., 2001)	Crowley and Unterman (2013)	(Sato et al., 1993)	(Stothers, 1996, 2001)	(Gao et al., 2008)
1653	25	–	0.0101	–	–	–	–
1654	–	–	0.0066	–	–	–	–
1655	–	–	0.0043	–	–	–	–
1656	–	–	0.0052	–	–	–	–
1657	–	–	0.0004	–	–	–	–
1658	–	–	0.0030	–	–	–	–
1659	–	–	0.0011	–	–	–	–
1660	340	–	0.0157	–	–	–	–
1661	255	0.341	0.0316	–	–	–	–
1662	170	–	–	0.013	–	–	–
1663	85	0.292	0.0024	0.004	–	–	–
1664	130	0.146	–	0.001	–	–	–
1665	100	–	0.0059	–	–	–	–
1666	65	0.112	0.0079	–	–	–	–
1667	30	0.089	0.0161	0.017	–	–	–
1668	–	–	0.0461	0.048	–	–	–
1669	–	–	–	0.011	–	–	–
1670	–	–	–	0.002	–	–	–
1671	–	–	0.0018	–	–	–	–
1672	200	–	0.0011	–	–	–	–
1673	150	0.168	0.0446	0.07	–	–	16.13
1674	100	–	0.0539	0.128	–	–	–
1675	50	–	0.0065	0.049	–	–	–
1676	–	–	0.0036	0.018	–	–	–
1677	–	–	–	0.007	–	–	–
1678	–	–	0.0001	0.001	–	–	–
1679	–	–	0.0051	–	–	–	–
1680	280	0.478	0.0008	0.021	–	–	–
1681	210	–	0.0001	0.018	–	–	–
1682	140	–	0.0007	0.007	–	–	–
1683	70	–	0.0065	0.002	–	–	–
1684	–	–	0.0009	0.001	–	–	–
1685	–	–	0.0019	–	–	–	–
1686	–	–	0.0080	0.006	–	–	–
1687	–	–	0.0020	0.003	–	–	–
1688	–	–	–	0.002	–	–	–
1689	–	–	0.0010	0.001	–	–	–
1690	–	–	–	–	–	–	–
1691	–	–	0.0005	–	–	–	–
1692	–	–	0.0106	–	–	–	–
1693	140	0.151	0.0563	–	–	–	27.1
1694	285	–	0.0777	0.105	–	–	–
1695	205	–	0.1405	0.158	–	–	–
1696	105	0.104	0.0395	0.171	–	–	–
1697	45	–	0.0028	0.075	–	–	–
1698	–	–	–	0.033	–	–	–
1699	–	–	0.0022	0.009	–	–	–
1700	–	–	0.0026	0.004	–	–	–
1701	–	–	0.0010	0.001	–	–	–
1702	–	–	–	0.002	–	–	–
1703	–	–	0.0003	–	–	–	–
1704	–	–	–	0.005	–	–	–
1705	–	–	0.0126	0.002	–	–	–

Table D1. Continued.

Year	N.H. DVI	N.H. AOD from paintings	AOD	AOD	AOD	AOD	Sulfate aerosols (Tg)
	(Lamb, 1970, 1977, 1983)	(this study)	(Robertson et al., 2001)	Crowley and Unterman (2013)	(Sato et al., 1993)	(Stothers, 1996, 2001)	(Gao et al., 2008)
1706	–	–	0.0040	0.004	–	–	–
1707	300	–	–	0.001	–	–	–
1708	225	–	–	–	–	–	–
1709	150	–	–	–	–	–	–
1710	75	0.104	0.0031	–	–	–	–
1711	–	–	0.0078	–	–	–	3.86
1712	80	–	0.0022	–	–	–	–
1713	60	–	0.0207	–	–	–	–
1714	40	–	0.0007	–	–	–	–
1715	20	–	0.0025	0.001	–	–	–
1716	–	–	0.0027	–	–	–	–
1717	120	–	0.0003	–	–	–	–
1718	90	0.13	0.0006	–	–	–	–
1719	60	–	0.0023	–	–	–	31.48
1720	30	0.058	0.0066	0.005	–	–	–
1721	100	–	0.0091	0.001	–	–	–
1722	75	–	0.0042	–	–	–	–
1723	50	–	0.0011	0.003	–	–	–
1724	55	–	–	0.001	–	–	–
1725	15	–	–	–	–	–	–
1726	15	–	0.0032	–	–	–	–
1727	15	0.087	0.0112	–	–	–	–
1728	15	–	0.0270	–	–	–	–
1729	15	–	0.0043	–	–	–	12.02
1730	160	0.126	0.0319	–	–	–	–
1731	130	–	0.0854	0.024	–	–	–
1732	90	–	0.0088	0.008	–	–	–
1733	50	–	–	0.002	–	–	–
1734	–	–	0.0002	–	–	–	–
1735	–	–	0.0012	–	–	–	–
1736	–	–	0.0006	–	–	–	–
1737	–	–	0.0044	–	–	–	–
1738	–	–	0.0122	–	–	–	3.34
1739	–	–	0.0167	0.017	–	–	–
1740	–	–	0.0359	0.035	–	–	–
1741	–	–	0.0032	0.008	–	–	–
1742	–	–	–	0.002	–	–	–
1743	–	–	–	–	–	–	–
1744	60	–	0.0012	–	–	–	–
1745	45	–	0.0079	–	–	–	–
1746	30	0.067	0.0009	–	–	–	–
1747	15	–	0.0200	0.005	–	–	–
1748	–	–	0.0001	0.001	–	–	–
1749	–	–	0.0154	–	–	–	–
1750	–	–	–	–	–	–	–
1751	–	–	0.0083	–	–	–	–
1752	200	–	0.0026	–	–	–	–
1753	150	0.167	0.0018	–	–	–	–
1754	160	–	0.0018	–	–	–	–
1755	255	–	0.0113	–	–	–	7.96
1756	150	–	0.0063	–	–	–	–
1757	95	–	0.0045	–	–	–	–
1758	40	–	0.0077	–	–	–	–

Table D1. Continued.

Year	N.H. DVI	N.H. AOD from paintings	AOD	AOD	AOD	AOD	Sulfate aerosols (Tg)
	(Lamb, 1970, 1977, 1983)	(this study)	(Robertson et al., 2001)	Crowley and Unterman (2013)	(Sato et al., 1993)	(Stothers, 1996, 2001)	(Gao et al., 2008)
1759	80	–	0.0029	–	–	–	–
1760	110	0.138	0.0015	0.005	–	–	–
1761	77	–	0.0072	0.001	–	–	12.91
1762	45	–	0.0116	0.024	–	–	–
1763	13	–	0.0074	0.007	–	–	–
1764	–	–	0.0028	0.002	–	–	–
1765	–	–	0.0028	–	–	–	–
1766	–	–	0.0136	–	–	–	–
1767	–	–	0.0035	–	–	–	–
1768	–	–	0.0002	–	–	–	–
1769	–	–	0.0056	–	–	–	–
1770	–	–	0.0041	–	–	–	–
1771	–	–	0.0012	–	–	–	–
1772	50	0.067	0.0029	0.006	–	–	–
1773	37	–	0.0034	0.002	–	–	–
1774	25	–	0.0003	–	–	–	–
1775	13	–	0.0051	–	–	–	–
1776	–	–	0.0032	–	–	–	–
1777	–	–	0.0002	–	–	–	–
1778	–	–	0.0011	0.005	–	–	–
1779	180	–	0.0015	0.006	–	–	–
1780	135	–	0.0019	0.001	–	–	–
1781	90	0.094	0.0092	–	–	–	–
1782	45	0.115	0.0106	–	–	–	–
1783	400	–	0.1643	0.009	–	–	92.96
1784	300	0.3	0.1354	0.042	–	–	–
1785	200	–	0.0005	0.01	–	–	–
1786	160	–	0.0021	0.002	–	–	–
1787	45	–	0.0080	–	–	–	–
1788	30	–	0.0035	0.011	–	–	–
1789	15	–	0.0011	0.003	–	–	–
1790	–	–	0.0022	0.001	–	–	–
1791	–	–	–	–	–	–	–
1792	–	–	0.0013	–	–	–	–
1793	–	–	0.0292	–	–	–	–
1794	–	–	0.0177	–	–	–	1.88
1795	120	0.098	0.0043	–	–	–	–
1796	130	–	0.0017	0.018	–	–	6.7
1797	90	–	0.0041	0.006	–	–	–
1798	50	–	0.0048	0.001	–	–	–
1799	130	–	0.0060	–	–	–	–
1800	90	–	0.0010	–	–	–	–
1801	60	0.081	0.0031	0.012	–	–	–
1802	30	–	0.0036	0.004	–	–	–
1803	–	–	0.0047	0.001	–	–	–
1804	–	–	0.0019	0.018	–	–	–
1805	–	–	0.0043	0.006	–	–	–
1806	–	–	0.0011	0.001	–	–	–
1807	–	–	0.0021	–	–	–	–
1808	–	–	–	–	–	–	–
1809	–	–	0.1391	0.198	–	–	53.74
1810	–	–	0.2308	0.18	–	–	–
1811	80	–	0.0537	0.067	–	–	–

Table D1. Continued.

Year	N.H. DVI	N.H. AOD from paintings	AOD	AOD	AOD	AOD	Sulfate aerosols (Tg)
	(Lamb, 1970, 1977, 1983)	(this study)	(Robertson et al., 2001)	Crowley and Unterman (2013)	(Sato et al., 1993)	(Stothers, 1996, 2001)	(Gao et al., 2008)
1812	180	0.199	0.0055	0.025	–	–	–
1813	170	0.181	0.0019	0.009	–	–	–
1814	170	0.142	0.0008	–	–	–	–
1815	695	–	0.3351	0.199	–	–	109.72
1816	490	0.6	0.3260	0.364	–	–	–
1817	375	0.379	0.0798	0.194	–	–	–
1818	195	0.33	0.0024	0.073	–	–	–
1819	30	0.108	0.0015	0.027	–	–	–
1820	15	0.062	0.0023	0.003	–	–	–
1821	–	–	0.0070	–	–	–	–
1822	200	–	0.0075	–	–	–	–
1823	150	–	0.0002	–	–	–	–
1824	100	–	0.0035	–	–	–	–
1825	70	0.104	0.0003	–	–	–	–
1826	80	0.15	0.0055	–	–	–	–
1827	65	0.143	0.0003	–	–	–	–
1828	50	0.147	0.0040	–	–	–	–
1829	75	0.147	0.0005	–	–	–	–
1830	50	0.069	0.0062	–	–	–	–
1831	200	0.293	0.0570	0.01	–	–	16.97
1832	130	0.284	0.0570	0.098	–	–	–
1833	80	0.16	–	0.048	–	–	–
1834	40	0.059	0.0081	0.018	–	–	–
1835	525	0.52	0.1300	0.127	–	–	40.16
1836	450	–	0.1527	0.116	–	–	–
1837	375	–	0.0218	0.042	–	–	–
1838	300	–	0.0091	0.015	–	–	–
1839	225	0.178	–	0.006	–	–	–
1840	150	0.185	0.0004	0.004	–	–	–
1841	75	0.11	0.0030	0.001	–	–	–
1842	–	–	0.0012	–	–	–	–
1843	–	–	0.0007	0.004	–	–	–
1844	–	–	0.0022	0.001	–	–	–
1845	100	0.145	0.0071	–	–	–	–
1846	205	–	0.0036	0.006	–	–	–
1847	140	–	0.0006	0.002	–	–	–
1848	90	–	0.0029	–	–	–	–
1849	30	–	0.0039	–	–	–	–
1850	–	–	–	–	0.0036	–	–
1851	–	–	–	–	0.0025	–	–
1852	–	–	0.0017	–	0.0014	–	–
1853	–	–	0.0075	–	0.0006	–	–
1854	–	–	0.0032	0.009	0.0003	–	–
1855	–	–	0.0043	0.004	0.0020	–	–
1856	140	–	0.0033	0.001	0.0387	–	–
1857	105	–	0.0014	–	0.0602	–	–
1858	70	0.098	0.0013	–	0.0290	–	–
1859	35	0.083	0.0001	–	0.0112	–	–
1860	–	–	–	0.003	0.0046	–	–
1861	160	0.164	0.0077	0.002	0.0034	–	4.23
1862	120	–	0.0075	0.054	0.0137	–	–
1863	80	–	0.0063	0.033	0.0100	–	–
1864	40	0.081	0.0067	0.012	0.0046	–	–

Table D1. Continued.

Year	N.H. DVI	N.H. AOD from paintings	AOD	AOD	AOD	AOD	Sulfate aerosols (Tg)
	(Lamb, 1970, 1977, 1983)	(this study)	(Robertson et al., 2001)	Crowley and Unterman (2013)	(Sato et al., 1993)	(Stothers, 1996, 2001)	(Gao et al., 2008)
1865	–	–	0.0037	0.005	0.0020	–	–
1866	–	–	0.0021	0.001	0.0008	–	–
1867	–	–	0.0018	–	0.0004	–	–
1868	160	0.204	0.0020	–	0.0002	–	–
1869	120	0.196	0.0013	–	0.0006	–	–
1870	80	–	0.0084	–	0.0006	–	–
1871	40	0.097	0.0009	–	0.0006	–	–
1872	–	–	0.0091	0.001	0.0013	–	–
1873	–	–	0.0033	0.008	0.0030	–	–
1874	–	–	0.0035	0.002	0.0020	–	–
1875	120	0.241	0.0012	0.01	0.0013	–	–
1876	90	–	0.0102	0.003	0.0062	–	–
1877	60	–	0.0130	0.001	0.0053	–	–
1878	30	0.143	0.0023	–	0.0032	–	–
1879	–	–	0.0009	–	0.0020	–	–
1880	–	–	–	–	0.0011	–	–
1881	–	–	–	–	0.0007	–	–
1882	–	–	–	–	0.0006	–	–
1883	400	0.56	0.0410	0.02	0.0473	0.096	21.87
1884	300	0.46	0.0897	0.157	0.1429	0.192	–
1885	240	0.361	0.0138	0.073	0.0635	0.071	–
1886	170	0.37	0.0302	0.045	0.0364	0.026	1.93
1887	50	0.21	0.0325	0.016	0.0371	–	–
1888	170	0.31	0.0036	0.004	0.0219	–	–
1889	125	–	0.0019	–	0.0285	–	–
1890	85	0.132	0.0031	0.004	0.0391	0.026	–
1891	45	0.101	0.0128	0.001	0.0300	0.048	–
1892	20	0.094	0.0090	0.004	0.0217	0.018	–
1893	15	0.108	0.0047	0.001	0.0094	–	–
1894	10	0.069	0.0007	–	0.0035	–	–
1895	5	–	0.0005	–	0.0014	–	–
1896	–	–	0.0011	–	0.0183	–	–
1897	–	–	0.0001	–	0.0169	–	–
1898	30	0.084	0.0041	0.007	0.0121	–	–
1899	25	0.084	0.0014	0.002	0.0046	–	–
1900	15	0.13	0.0027	–	0.0018	–	–
1901	5	–	0.0021	–	0.0007	–	–
1902	180	0.27	0.0094	0.004	0.0202	0.014	3.77
1903	135	–	0.0478	0.069	0.0715	0.118	–
1904	90	0.118	0.0092	0.038	0.0318	0.061	–
1905	45	–	0.0032	0.014	0.0126	–	–
1906	–	0.17	0.0049	0.005	0.0073	–	–
1907	60	0.2655	0.0078	0.013	0.0092	0.01	–
1908	45	0.2	0.0056	0.006	0.0103	0.004	–
1909	30	0.13	–	0.001	0.0040	–	–
1910	15	–	0.0008	–	0.0031	–	–
1911	–	–	0.0518	–	0.0017	–	–
1912	60	0.163	0.0161	0.031	0.0193	0.028	11.04
1913	45	0.16	0.0120	0.029	0.0241	0.019	–
1914	30	0.168	0.0048	0.006	0.0099	0.007	–
1915	15	0.106	0.0055	0.001	0.0039	–	–
1916	–	0.177	0.0040	0.009	0.0027	–	–
1917	–	0.122	0.0016	0.003	0.0022	–	–

Table D1. Continued.

Year	N.H. DVI	N.H. AOD from paintings	AOD	AOD	AOD	AOD	Sulfate aerosols (Tg)
	(Lamb, 1970, 1977, 1983)	(this study)	(Robertson et al., 2001)	Crowley and Unterman (2013)	(Sato et al., 1993)	(Stothers, 1996, 2001)	(Gao et al., 2008)
1918	–	0.12	0.0036	0.001	0.0020	–	–
1919	–	0.195	0.0072	–	0.0020	–	–
1920	–	0.16	0.0014	–	0.0094	–	–
1921	–	0.156	0.0012	0.005	0.0077	–	–
1922	–	0.2	0.0052	0.001	0.0029	0.008	–
1923	–	0.13	0.0031	–	0.0011	0.004	–
1924	–	–	0.0102	0.011	0.0034	–	–
1925	–	0.15	0.0106	0.005	0.0029	–	11.15
1926	–	–	0.0126	0.001	0.0023	–	–
1927	–	0.175	0.0029	–	0.0015	–	–
1928	–	0.195	0.0036	–	0.0053	0.002	–
1929	–	–	0.0029	0.002	0.0098	0.014	–
1930	–	–	0.0002	0.002	0.0062	–	–
1931	–	–	0.0075	0.006	0.0047	–	–
1932	–	0.161	0.0005	0.01	0.0082	0.012	–
1933	–	0.172	0.0026	0.003	0.0067	0.002	–
1934	–	–	0.0028	0.001	0.0038	–	–
1935	–	0.116	0.0058	–	0.0042	–	–
1936	–	0.122	0.0021	–	0.0033	–	–
1937	–	–	0.0278	–	0.0028	–	–
1938	–	0.136	0.0044	–	0.0049	–	–
1939	–	–	0.0054	–	0.0041	–	–
1940	–	0.094	0.0004	–	0.0032	–	–
1941	–	–	0.0050	–	0.0019	–	–
1942	–	–	0.0036	–	0.0042	–	–
1943	–	0.094	0.0728	–	0.0044	–	6.61
1944	–	0.21	0.0499	–	0.0024	–	–
1945	–	–	0.0012	–	0.0022	–	–
1946	–	–	0.0033	–	0.0018	–	–
1947	–	–	0.0056	–	0.0023	–	–
1948	–	–	0.0033	–	0.0017	–	–
1949	–	–	0.0029	–	0.0033	–	–
1950	–	–	0.0027	–	0.0029	–	–
1951	–	–	0.0507	–	0.0020	–	–
1952	–	0.167	0.0559	–	0.0037	–	–
1953	–	0.268	0.0056	–	0.0034	–	–
1954	–	–	0.0006	–	0.0036	–	–
1955	–	–	0.0038	–	0.0018	–	–
1956	–	–	0.0068	0.005	0.0011	–	–
1957	–	–	0.0053	0.001	0.0005	–	–
1958	–	0.293	0.0008	–	0.0003	–	–
1959	–	–	0.0029	–	0.0002	–	–
1960	–	–	0.0005	–	0.0046	–	–
1961	–	–	0.0053	–	0.0108	–	–
1962	–	–	0.0024	–	0.0133	0.012	–
1963	160	–	0.0502	0.04	0.0460	0.066	17
1964	120	–	0.0389	0.055	0.0717	0.051	–
1965	80	–	0.0149	0.03	0.0432	0.031	–
1966	40	–	0.0027	0.01	0.0232	0.014	–
1967	31.4	0.138	0.0053	0.003	0.0145	0.019	–
1968	60.7	0.32	0.0164	0.001	0.0274	0.011	–
1969	40	–	0.0388	–	0.0344	0.006	–
1970	32.4	–	0.0275	–	0.0166	0.006	–

Table D1. Continued.

Year	N.H. DVI	N.H. AOD from paintings	AOD	AOD	AOD	AOD	Sulfate aerosols (Tg)
	(Lamb, 1970, 1977, 1983)	(this study)	(Robertson et al., 2001)	Crowley and Unterman (2013)	(Sato et al., 1993)	(Stothers, 1996, 2001)	(Gao et al., 2008)
1971	23.7	–	0.0141	–	0.0065	0.015	–
1972	9.5	–	0.0135	–	0.0039	0.008	–
1973	9.3	–	0.0047	–	0.0078	0.001	–
1974	56.1	–	0.0055	–	0.0127	0.007	–
1975	41	–	0.0071	0.024	0.0301	0.024	–
1976	67	–	0.0080	0.015	0.0136	0.007	4.72
1977	45.4	–	–	0.006	0.0051	0.003	–
1978	25.8	–	0.0051	0.002	0.0075	0.001	–
1979	25.4	0.19	0.0019	0.001	0.0092	–	–
1980	51	–	0.0010	–	0.0047	–	–
1981	41	–	0.0098	–	0.0050	–	–
1982	366.1	–	0.0492	0.048	0.0525	–	14
1983	267.2	–	0.0370	0.079	0.0752	–	–
1984	171.1	0.19	–	0.03	0.0302	–	–
1985	85	–	–	0.011	0.0126	–	–
1986	–	–	–	0.004	0.0136	–	–
1987	–	–	–	–	0.0103	–	–
1988	–	–	–	–	0.0076	–	–
1989	–	–	–	–	0.0061	–	–
1990	–	–	–	–	0.0061	–	–
1991	–	0.15	–	0.037	0.0539	–	30.1
1992	–	–	–	0.131	0.1211	–	–
1993	–	–	–	0.053	0.0490	–	–
1994	–	–	–	0.02	0.0200	–	–
1995	–	–	–	0.007	0.0096	–	–
1996	–	0.22	–	0.001	0.0065	–	–
1997	–	–	–	–	0.0052	–	–
1998	–	–	–	–	0.0028	–	–
1999	–	–	–	–	0.0021	–	–
2000	–	–	–	–	0.0021	–	–